5

Collisional Evolution of Dust Aggregates; from Compaction to Catastrophic Destruction.

D. Paszun and C. Dominik
Submitted to Astronomy & Astrophysics

Abstract
The coagulation of dust aggregates occurs in various astrophysical environments. Each one is characterized by different conditions that influence the growth (e.g.,relative velocities, composition and size of smallest constituents - monomers). Here we study the microphysics of collisions of dust aggregates in a four dimensional parameter space (parameters are: the collision energy, the initial compactness of agglomerates, the mass ratio of collision partners, and the impact parameter). For this purpose we employ a state of the art *molecular dynamics* type of model that has been extensively and successfully tested against laboratory experiments. It simulates the motion of individual monomers interacting dynamically via surface, van der Waals forces. The structure of aggregates is quantified by the filling factor that provides both the information about the internal structure (packing density of monomers) and the projected surface of aggregates.
Our results show a significant importance of the impact parameter that causes formation of elongated particles, due to tensile forces acting in offset collisions. In head-on impacts aggregates are compacted at lower energies. A sufficient energy causes the restructuring to reach the maximum compaction. If more energy is provided, pancake-like structures are formed. We find that the outcome of collisions can be represented in a simple way. A highly pronounced large fragment component coexists with a power-law distribution of small fragments. Moreover the structural parameter of these small fragments is very well described by a simple relation, regardless of the initial compactness, impact energy or impact parameter. The simulations show that erosion by collisions with large mass ratio can be significant (the ejected mass can be a few orders of magnitude larger than the mass of smaller impactor) at relatively small energies, compared to collisions of equal mass aggregates, where the same energies can lead to perfect sticking.
These findings are summarized in a form of a simple collision recipe. This recipe provides the outcome of a collision averaged over the impact parameter and is provided in tabulated form for a range of physical quantities (energy, filling factor). The mass ratio effect is taken into account by providing the local and the global recipes that describe collisions of very different and similar masses, respectively.

5.1 Introduction

It is commonly accepted that planets form in disks around young stars by collisional accumulation of dust particles. Initially very small grains, well coupled to the gas in a disk, collide at very low velocities and stick due to the Van der Waals forces (Johnson et al. 1971; Derjaguin et al. 1975). At this very first steps of planet formation the main source of relative velocities is the Brownian motion. In the absence of fragmentation, this so called Brownian growth preferentially collides particles of similar size, leading to the formation of fractal aggregates (Kempf et al. 1999; Blum et al. 2000; Krause and Blum 2004; Paszun and Dominik 2006). Fractals produced by Brownian growth have the fractal dimension $D_\mathrm{f} = 1.5$ (Krause and Blum 2004; Paszun and Dominik 2006), higher gas densities shorten the mean free path of particles and results in even more fluffy structures. In the limiting case, aggregates formed this way may be very elongated with the fractal dimension approaching unity (Paszun and Dominik 2006).

The growth of dust to bigger sizes results eventually in decoupling of aggregates from the gas. Since the gas component moves at sub–Keplerian velocity, dust particles are exposed to a head wind, which results in a drag force. This leads to a radial drift of dust, which eventually ends up in an evaporation region close to the star. The drift velocity depends on the size of an aggregate. Weidenschilling (1977) showed that meter sized particles may fall into the central star within only 100 orbits.

Aggregates that decouple from the gas are also more difficult to be mixed upward. Thus small particles that grew to larger sizes in the upper parts of the disk, once decoupled they start to settle to the midplane sweeping other aggregates on their way down.

Particles may also be trapped in turbulent eddies resulting in collisions between aggregates of different size. An aggregate of a given size (in Epstein regime) respond to the gas drag within a friction time (sometimes also referred to as stopping time) given by

$$\tau_\mathrm{f} = \frac{3}{4 c_\mathrm{g} \rho_\mathrm{g}} \frac{m}{\sigma}, \tag{5.1}$$

where c_g and ρ_g are,respectively, the sound speed and the volume mass density of the gas, and m and σ are the mass and the projected surface of the particle. Thus aggregates with different τ_f have different velocities. The bigger the friction time difference between two particles, the higher the relative velocity is (Voelk et al. 1980; Weidenschilling and Cuzzi 1993; Ormel and Cuzzi 2007).

Initially low impact velocities result in sticking of aggregates. However, the growth of dust and the resulting decoupling of particles cause an increase of collision velocities. When the collision energy becomes higher than the energy needed to roll monomers over each other (later referred to as rolling energy E_roll), restructuring begins. Very fluffy and fractal aggregates are compacted upon collision (Dominik and Tielens 1997; Blum and Wurm 2000). An increase

of the impact velocity leads to stronger compaction. However, eventually the kinetic energy is high enough to break contacts between individual monomers. Erosion starts to remove parts of colliding aggregates. As the relative velocity increases, erosion also becomes stronger, leading ultimately to a destruction of the aggregates.

The fragmentation of aggregates is a major problem in planet formation theory. Dust cannot grow all the way to form planetesimals because it gets destroyed once relative velocities become violent enough to disrupt aggregates. Similarly the radial drift may prevent growth by removing particles from the disk once they grow to a certain size and spiral towards the central star dramatically fast.

Johansen et al. (2006b) showed that in the presence of turbulence planetesimals might be produced by a gravitational collapse of clumps of meter sized boulders. These clumps are generated by high pressure turbulent eddies that trap and concentrate the particles, which then become gravitationally bound. Before this process can take place, particles must already have grown by 18 orders of magnitude in mass. The only feasible way to do that is by collisional sticking. Because collisional fragmentation of aggregates may prevent growth of large, meter sized aggregates, it is crucial to fully understand mechanisms involved in collisions of porous aggregates.

Blum and Wurm (2000) performed laboratory experiments of collisions of dust aggregates. They studied impacts at a wide range of energies, from low energy (perfect sticking), through restructuring to fragmentation of microscopic aggregates. Their results as to restructuring threshold are in agreement with theoretical findings of Dominik and Tielens (1997). The fragmentation energy, however, differs, which is a result of discrepancy in sticking velocity. Poppe et al. (2000) determined the sticking velocity of a micron sized silica grain, experimentally, to be 1.2 m/s. Chokshi et al. (1993) and Dominik and Tielens (1997) on the other hand derived theoretically a much lower velocity, inconsistent with experiments.

Blum and Muench (1993) studied collisions of macroscopic, mm–sized, aggregates at velocities between 1 and a few m/s. In this case, however, a different behavior was observed. Although particles were very porous (up to 4% filling factor) they did not observe restructuring. Instead aggregates were bouncing off each other or, for faster impacts, fragmenting.

Very energetic collisions between large mm–sized and cm-sized aggregates were studied by Wurm et al. (2005b). They showed that the fragmentation observed at high velocity impacts turns into a net growth of 50% at velocities above 13 m/s. The distribution of fragments at velocities of about 20 m/s followed a power-law with a slope of -5.6 ± 0.2 for larger fragments and was flat for the smallest ejecta.

Fujiwara et al. (1977) experimented with solid basalt rocks. High velocity impacts of the order of a few km/s result in a power-law distribution of small fragments $n(m) \sim m^k$. The slope of the distribution was found to be $k = -1.83$.

They distinguished several collisional outputs, depending on the target size:

1. complete destruction;
2. remaining core;
3. transition from core to cratering;
4. crater formation.

Sirono (2004) has developed a smoothed particles hydrodynamics (SPH) model to simulate meter sized and larger aggregates. A single particle in this model corresponds to a porous material described by compressive strength, tensile strength, density, and sound speed. This method was also used by Schäfer et al. (2007).

Although collisions of dust particles have been studied experimentally and theoretically, no one has formulated a quantitative, two dimensional (because it provides both size distribution and structure of particles) recipe describing the collisional output and based on empirical results. Both the distribution of masses and the compactness of fragments is required to fully understand the growth of dust. Here we present an extensive parameter study of many collisions of small dust aggregates. We provide the recipe for mass distribution and compactness of fragments.

In Sect. 5.2 we briefly present the model we adopt to simulate collisions of dust aggregates. Then in Sect. 5.3 we describe the parameter space and collision setup. Section 5.4 provides quantities we use to describe an outcome of collisions and expected energy scaling. Our results presented in Sect. 5.5 are followed by the collision recipe (Sect. 5.6). The discussion of our results and of the recipe is given in Sect. 5.7. We end this paper with interesting conclusions in Sect. 5.8.

5.2 The Model

The simulations presented in this work are done using the N-body dynamics code SAND. Our model treats all monomers (also referred to as grains or particles) in the agglomerates (also referred to as aggregates, clusters, or particles) individually. Since we are currently not interested in long range interactions, electrostatic, magnetic and gravitational forces are not included even though the code can handle them (Dominik and Nübold 2002). We calculate motion of individual monomers that interact with each other via attractive Van der Waals surface force (Johnson et al. 1971).

The presence of the attractive surface inevitably leads to several energy dissipation mechanisms. The particles, when in contact, may roll over each other. This rolling motion is opposed by a rolling friction force (Dominik and Tielens 1995) causing the energy loss. The same happens in the case of a sliding motion. The contacts may shift which again is work done against the sliding friction

force (Dominik and Tielens 1996). Beside that, every time a contact between two monomers is broken, the elastic energy stored in it is partially lost (Johnson et al. 1971; Chokshi et al. 1993; Dominik and Tielens 1997). Some energy may also be lost due to a twisting motion of particles in contact (Dominik and Tielens 1997).

We also include an additional energy dissipation channel in order to fit the experimental results by Poppe et al. (2000). This process increases the sticking velocity from about $10\,\mathrm{cm\,s^{-1}}$ (Chokshi et al. 1993; Dominik and Tielens 1997) to about $1\,\mathrm{m\,s^{-1}}$ (Poppe et al. 2000). Since the measured attractive force agrees well with the theory provided by Johnson et al. (1971) and Derjaguin et al. (1975), the difference in sticking velocity points to additional energy losses in collisions. While our model does not specify what this mechanism is, a candidate would be plastic deformation of surface asperities on nm scales. In order to achieve agreement with the experimental results, a mechanism dissipating the energy upon the first contact of two particles was introduced (Paszun and Dominik 2008b).

Paszun and Dominik (2008b) tested the model extensively against the laboratory experiments and found a good agreement. For details regarding the implementation, we refer the reader to Dominik and Nübold (2002) and Paszun and Dominik (2008b).

5.3 The Setup

To provide a qualitative and quantitative description of aggregates collisions, we explore an extensive parameter space. This provides an insight into the effects of different parameters on the outcome of a collision. As the final purpose is to provide a recipe for a collision between two aggregates, we limit the range of our parameters to realistic values.

We believe the main parameters influencing the outcome of a collision are:

- collision energy,
- pre-collision compactness of the aggregate,
- mass ratio of colliding particles,
- impact parameter,
- material properties.

The influence of each parameter is discussed in detail in Sect. 5.4.

The range of our parameter space is presented in Tab. 5.1. However, not all combinations of these parameters are sampled. We cover the energy range from the hit-and-stick (no restructuring) regime up to catastrophic destruction (all mass turns into small fragments) for several particle masses. Due to limit of the computational power and the large number of long-lasting simulations, we limit the size of our aggregates to maximum of 1000 monomers. This allows

Table 5.1 — Parameters explored in this study. Although not all combinations are simulated, each one that is, is done for 6 different orientations in order to obtain an average collision output. Columns correspond to (1)-relative collision velocity v, (2)-mass of an aggregate m, (3)-pre-collision filling factor of an aggregate ϕ_σ(see text), (4)-impact parameter $b/b_{\max}$, (5)-mass ratio of colliding aggregates m_1/m_2.

v [m/s]	m/m_0	ϕ_σ	$b/b_{\max}$	m_1/m_2
(1)	(2)	(3)	(4)	(5)
0.01	1	0.07	0.0	10^{-3}
0.05	50	0.09	0.25	$5 \cdot 10^{-2}$
0.1	100	0.122	0.5	$1 \cdot 10^{-1}$
0.2	200	0.13	0.75	$2 \cdot 10^{-1}$
0.3	400	0.155	0.875	$4 \cdot 10^{-1}$
0.5	600	0.16	0.95	$6 \cdot 10^{-1}$
0.75	800	0.189		$8 \cdot 10^{-1}$
1.0	1000	0.251		1
2.0				
4.0				
6.0				
8.0				
10.0				

us to sample the mass ratio within the range from $m_1/m_2 = 1$ down to $m_1/m_2 = 10^{-3}$. Moreover, we perform a large number of simulations of collisions between aggregates of equal mass, made of 200, 400, and 1000 monomers. Each collision for each set of parameters is computed for 6 different relative orientations, to average over effects caused by the non-spherical, inhomogeneous structure of the individual aggregates. This provides a spread in possible outcomes of a collision.

The sampling of the impact parameter b covers the entire possible range from a central impact, up to a grazing collision, where the impact parameter b equals 95% of the sum of the outer radii of two colliding aggregates $R_{\text{out},1} + R_{\text{out},2}$.

For the compactness parameter we use the filling factor ϕ_σ defined as

$$\phi_\sigma = N\left(\frac{r_0}{R_\sigma}\right)^3, \tag{5.2}$$

where N is the number of monomers in the aggregate, r_0 is a monomer radius, and R_σ is the projected surface equivalent radius (cf. Fig. 5.1) and is defined as

$$R_\sigma = \sqrt{\frac{\sigma}{\pi}}, \tag{5.3}$$

with σ being the projected surface averaged over many orientations. The inverse of the filling factor was introduced by Ormel et al. (2007) as the enlargement factor ψ. Although our work samples a limited range in ϕ_σ, this is physically justified. The most compact aggregate made of equal size monomers is

represented by the close cubic packing (CCP). In this case the filling factor is about[1] $\phi_\sigma \approx 0.74$. Such aggregates, however, cannot result from a collision process. Random close packing (RCP) of spheres is produces aggregates with the filling factor of about $\phi_\sigma \approx 0.635$ (Onoda and Liniger 1990) that is somewhat lower. However, Blum et al. (2006) and later Paszun and Dominik (2008b) show that aggregates being compressed reach maximum filling factor of about $\phi_\sigma = 0.33$. Higher compaction cannot be reached in a static experiment of uniaxial compression, as monomers move sideways increasing the tangential size with further compression. Therefore as the upper limit for the filling factor of aggregates we use a slightly lower value of $\phi_\sigma = 0.25$. The lower limit, on the other hand, we set for fractal aggregates. The Brownian growth in the presence of rotation forms aggregates of very open structure with the fractal dimension of about $D_\mathrm{f} = 1.5$ (Krause and Blum 2004; Paszun and Dominik 2006). Our largest aggregate of the fractal dimension 1.5 has the filling factor $\phi_\sigma = 0.07$.

A few examples of our aggregates, made of 1000 monomers, are presented in Fig. 5.1. These particles are made of equal size monomers. They are constructed

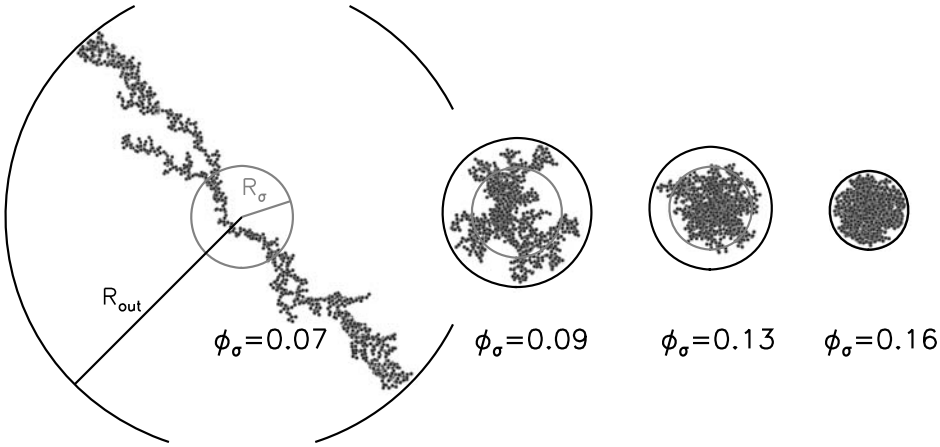

Figure 5.1 — Sample aggregates as used in our parameter study. Each of particles is made of 1000 monomers. Annotations show $\phi_\sigma$for each particle. Black circle defines the outer radius R_out, while the grey circles indicate the projected surface equivalent radius R_σ (see text).

using two different techniques. The first method developed by Filippov et al. (2000), allows to create fractal aggregates of any specified fractal dimension D_f. This sequential tunable particle-cluster aggregation method forms agglomerates by successive addition of identical spherical particles. The fractal aggregates made according to this algorithm exactly obey the scaling law (Filippov et al.

[1] Although the value of 0.74 correspond to filling factor defined in respect to the outer radius R_out and not R_σ, both radii are equal for these compact aggregates.

2000)

$$N = k_{\rm f}\left(\frac{R_{\rm g}}{r_0}\right)^{D_{\rm f}}, \tag{5.4}$$

where $R_{\rm g}$ is the radius of gyration and $k_{\rm f}$ is the fractal pre-factor that is related to the central packing density. For the aggregates used in our study, we choose a pre-factor $k_{\rm f} = 1.6$ and fractal dimensions of $D_{\rm f} = 1.5$, $D_{\rm f} = 2.0$, and $D_{\rm f} = 2.5$. In the case of $N = 1000$ this results in the filling factor $\phi_\sigma = 0.07$, $\phi_\sigma = 0.09$, and $\phi_\sigma = 0.16$, respectively.

The second method we use to produce aggregates is particle cluster aggregation (PCA). We successively add monomers from random directions. This produces aggregates that, in the limit of very large sizes, have a filling factor of $\phi_\sigma = 0.15$. An aggregate made of 1000 monomers has, however, a smaller filling factor of $\phi_\sigma = 0.13$. This is an effect of high porosity of the surface layer. In very large aggregates, this region will be negligibly thin compared to the size of an aggregate (Paszun et al. 2008).

It is important to note the discrepancy between the radii used in the definition of the impact parameter space and the filling factor ϕ_σ. The impact parameter is defined in terms of the outer radius $R_{\rm out}$, that is the radius of a sphere enclosing an entire aggregate and centered in its center of mass. The filling factor, however, uses the projected surface equivalent radius R_σ. For compact aggregates these two radii are very similar, while the outer radius $R_{\rm out}$ becomes higher as the filling factor of an aggregate decreases. For completeness, we empirically determine the relation between the two radii. Figure 5.2 shows how this ratio ($R_{\rm out}/R_\sigma$) influences the filling factor ϕ_σ. To obtain this relation we constructed (using Eq. (5.4)) many aggregates of different structure ($D_{\rm f}$, $k_{\rm f}$) and mass (N). Interestingly all data is very well confined along a simple curve. As the filling factor seems to depend on the mass of aggregate as $\phi_\sigma \propto N^{-0.33}$, we plot $\phi_\sigma N^{0.33}$ in Fig. 5.2 to collapse all data on a single curve. This mass dependence is further discussed in Sect. 5.5.2 and Sect. 5.5.3. Compact particles in Fig. 5.2 ($R_{\rm out}/R_\sigma < 1.2$) have similar outer radius $R_{\rm out}$ and the projected surface equivalent radius R_σ and they show little dependence of the $R_{\rm out}/R_\sigma$ ratio on the filling factor. Fluffy aggregates ($R_{\rm out}/R_\sigma > 1.2$) on the other hand show a power-law relation of the filling factor on the ratio of the two radii with a slope of −0.3. The fitted power-law is presented in Fig. 5.2 as dashed-dotted line. The complete relation that holds for ratio $R_{\rm out}/R_\sigma > 1.2$ is given as

$$\phi_\sigma = 1.21\left(\frac{R_{\rm out}}{R_\sigma}\right)^{-0.3} N^{-0.33}. \tag{5.5}$$

Although material properties play a major role in collisions of dust aggregates, we focus in this study on a single species. The physical parameters of Silica used in our model are presented in Tab. 5.2. Other materials will be subject of future study. Our monomers are silica spheres with a diameter of 1.2

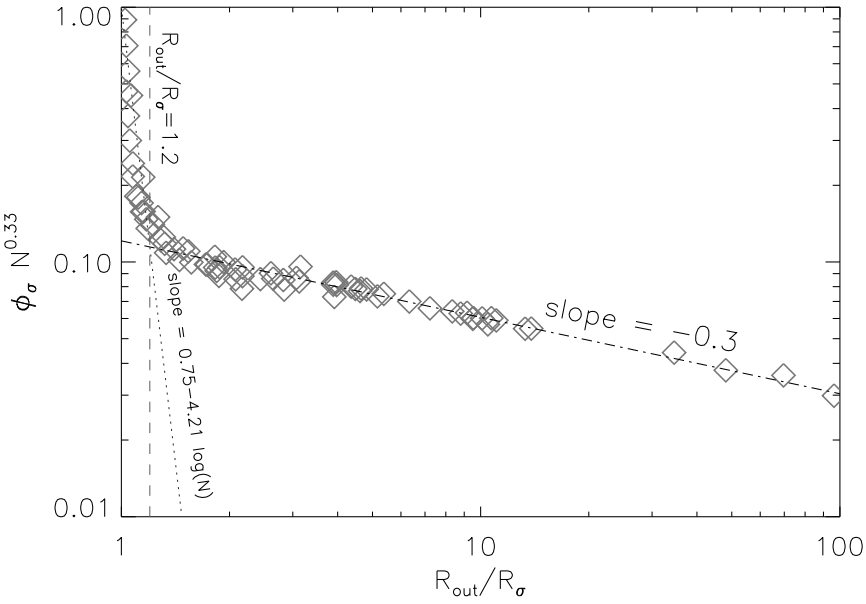

Figure 5.2 — The filling factor as a function of the ratio $R_{\rm out}/R_\sigma$ of the outer radius of an aggregate over its projected surface equivalent radius. Each point corresponds to an aggregate (see text) of different structure and mass and thus different ratio of the two radii. The dashed-dotted line shows the least square fit of the power-law to this data. A sharp transition between compact and fluffy particles occurs at about $R_{\rm out}/R_\sigma \approx 1.2$ (dashed line). Compact aggregates have smaller ratio of the two radii. Their filling factor is approximated by a power-law (dotted line).

micron. The elasticity modulus E^* is defined as

$$E^* = \left(\frac{1-\nu_1^2}{E_1} + \frac{1-\nu_2^2}{E_2} \right)^{-1}, \tag{5.6}$$

where E_i and ν_i are the Young's modulus and the Poisson ratio of i-th monomer, respectively.

5.4 Measuring the structure of aggregates and the effect of collisions

Here we present quantities that are further used to quantify the structure of aggregates and outcome of a collision.

Table 5.2 — Properties of monomers used in this study. Material properties correspond to Quartz monomers or radius $r_0 = 6 \cdot 10^{-5}$ cm.

γ [erg/cm^2]	E^* [dyn/cm^2]	$\xi_{\rm crit}$ [cm]	ρ [g/cm^3]
25	$2.78 \cdot 10^{11}$	$2 \cdot 10^{-7}$	2.65

5.4.1 Structure of an aggregate

The structure of an aggregate can be described by several quantities. However, it is difficult to fully characterize the structure by a single parameter. Here we present several quantities and briefly discuss their relevance.

Number of contacts

The strength of an aggregate can very well be expressed in terms of contacts between monomers. The more contacts there are in the aggregate, the more stable and resistant against restructuring it is. In a typical CCA aggregate the number of contacts is equal to the number of grains, meaning that most monomers (except those at the end of chains) have two contacts with neighboring monomers. Thus such a structure can be easily restructured. The aggregate can be stretched or compacted. Monomers in the cores of the densest aggregates can have a maximum of 12 contacts (the case of the close cubic packing). However, aggregates in which the number of contacts divided by the number of monomer is 2 or more are already very strong and can resist restructuring very well. In this case every monomer in the center of the particle is attached to three others, effectively preventing rolling motion of monomers. Although it is a very appropriate way to describe the strength of an aggregate, it has few useful applications. The structure of an aggregate is needed to be known in order to properly describe interaction of the aggregate with the surrounding matter. The gas drag force exerted onto particles depends on the cross section of the particles. Since number of contacts $N_{\rm cont}$ in an aggregate can not be directly translated into a unique cross section, it is better to make use of different quantity that is related to the cross section more closely.

Fractal dimension

The fractal dimension defined in Eq. (5.4) describes the density profile of an aggregate. It cannot fully describe the structure of an aggregate alone. For a complete description the knowledge of the prefactor ($k_{\rm f}$) is required, which determines packing density in the particle.

Geometrical filling factor

A very intuitive way of describing an aggregate in terms of the structure is to provide the packing density. Low values are immediately associated with ineffi-

cient packing, low density and a weak structure. A larger filling factor indicates close packing, many contacts and higher strength. A proper definition of the filling factor provides a number of advantages. In this work we adopt the *geometrical* filling factor defined in eq. 5.2. It describes the structure of an aggregate in an intuitive way and carries additional information about the projected surface. Therefore, the friction time may be easily determined for such aggregates.

5.4.2 Effect of collisions

Quantities defined in the previous sections can now be used to describe possible structural changes of aggregates that may occur during a collision. We also present the expected scaling that is useful to comprehend the results of the extensive parameter study.

Basic scaling

Aggregates made of a large number of monomers may dissipate energy through several mechanisms like rolling of breaking. Therefore, larger clusters may dissipate more energy, as the amount of monomer-monomer interactions is larger. Thus, intuitively if provided energy is sufficient to break all connections in colliding aggregates, shattering should occur. It is then useful to scale the energy with the number of contacts N_c.

More applicable scaling, however, is a number of particles N, as it is comparable to the number of contact and does not change during a collision. This is not affected during an impact, contrary to the number of contacts. Therefore we adopt scaling with the number of monomers N.

Influence of the impact energy

Dominik and Tielens (1997) and later Wada et al. (2007) provide a simple recipe of collisional output as a function of energy. Both these studies were limited to two dimensional aggregates. Their recipe predicts energy thresholds for processes like erosion, compression and fragmentation. To understand them, one needs to define the rolling energy and the breaking energy of a contact. The first one is the energy needed to roll two monomers over each other by 90 degrees, and represents the energy related to restructuring of an aggregate. It is defined as (Dominik and Tielens 1997)

$$E_{\mathrm{roll}} = 6\pi^2 \gamma R \xi_{\mathrm{crit}}, \tag{5.7}$$

where γ is a surface energy, R is reduced radius of the two monomers in consideration, and ξ_{crit} is a critical displacement, at which the rolling becomes irreversible and energy is dissipated. This quantity is of the order of 20Å as shown by Heim et al. (1999). The second energy is the energy needed to separate two connected monomers and is defined as

$$E_{\mathrm{br}} = 1.8 F_c \delta_c. \tag{5.8}$$

Table 5.3 — The collision recipe from Dominik and Tielens (1997) for a 2D case.

Energy	Outcome of Collision
$E_{\rm impact} < 5E_{\rm roll}$	Sticking without restructuring
$E_{\rm impact} \approx 5E_{\rm roll}$	Onset of restructuring local to the impact area
$E_{\rm impact} \approx n_{\rm c}E_{\rm roll}$	Maximum compression
$E_{\rm impact} \approx 3n_{\rm c}E_{\rm br}$	Onset of erosion (start to lose monomers)
$E_{\rm impact} > 10n_{\rm c}E_{\rm br}$	Catastrophic disruption

Here $F_{\rm c}$ is a pull-off force, minimum force needed to disconnect two monomers and it is

$$F_{\rm c} = 3\pi\gamma R. \tag{5.9}$$

$\delta_{\rm c}$ is the critical displacement from the equilibrium position (Dominik and Tielens 1997). Thus two monomers in contact at this position will disconnect if pulled. $\delta_{\rm c}$ is defined as

$$\delta_{\rm c} = \frac{1}{2}\frac{a_0^2}{6^{1/3}R}, \tag{5.10}$$

with the equilibrium contact radius

$$a_0 = \left(\frac{9\pi\gamma R^2}{E^*}\right)^{1/3}. \tag{5.11}$$

Putting these equations together we see that the critical energy is given by

$$E_{\rm br} = A\frac{\gamma^{5/3}R^{4/3}}{E^{*2/3}}, \tag{5.12}$$

with the dimensionless constant $A = 43$.

The recipe of Dominik and Tielens (1997) is confirmed experimentally with one important modification (Blum and Wurm 2000). The energy scaling should be applied according to values determined empirically (i.e. $\xi_{\rm crit} \approx 20$Å and $E_{\rm br}$ corresponding to the experimental results). In order to satisfy this requirement we introduce a scaled version of $E_{\rm br}$. In this case the constant A is higher, such that the sticking threshold in our model is in agreement with experiments (Poppe et al. 2000). This energy is given by

$$E_{\rm br} = 2.8 \cdot 10^3\frac{\gamma^{5/3}R^{4/3}}{E^{*2/3}}. \tag{5.13}$$

The recipe by Dominik and Tielens (1997) is summarized in Tab. 5.3. Low energies are insufficient to cause any visible restructuring. Before any restructuring occurs, contact between monomers are displaced elastically and only the critical displacement causes an irreversible motion (i.e.,rolling or sliding). When

the energy suffices to roll several contacts by a significant angle (~90 degrees), monomers in the impact region begin to roll and visible restructuring occurs. As the energy increases more restructuring occurs. The maximum compression is reached, when all monomers have enough energy to roll by 90 degrees.

Monomers begin to break out of an aggregate when the energy per contact reaches 3 times the breaking energy. A large fraction of the energy is then dissipated by rolling but the excess is used to remove a few grains. As the impact energy increases the erosion increases and becomes catastrophic when each contact can access over 10 times the breaking energy.

Although this recipe is reasonable, it may differ when particles collide at an impact parameter other than $b = 0$ or when the mass ratio of the two collision partners is not 1. The latter case was also considered by Dominik and Tielens (1997). They provided a recipe for collisions of a small grain with a cluster.

Influence of fluffiness

The structure of colliding aggregates can strongly affect the distribution of the collision energy within aggregates. In fluffy particles with loosely packed monomers breaking a single contact can reduce the size of an aggregate by a factor of 2. Therefore, in collisions that involve open particles a smaller number of monomers actively participate in the distribution and dissipation of the energy. For example a collision of two linear chains involves only a few grains, as the energy is used to break several contacts, local to the impact site. Larger fragments are detached and become unavailable for any further interaction concerning this particular collision event.

Compact aggregates are characterized by a higher packing density of monomers, which results in the energy distribution over a larger number of grains. Even if a few contacts are broken, monomers cannot easily escape the aggregates. Moreover, the energy is transported faster within the particles, as the sound speed in porous aggregate is an increasing function of the packing density (Paszun and Dominik 2008b).

Influence of the mass ratio

Impact of particles of different mass may lead to a different collision output than in the case of equal masses. Smaller projectiles have limited area over which the impact energy is transferred into the target. The interaction is local and thus fewer contacts and particles will be involved in such a collision. Thus a collision between similar mass clusters should result in more efficient distribution of energy between monomers of both particles.

The mass ratio influence may strongly depend on the fluffiness of aggregates under consideration. In the case of fluffy aggregates, however, small projectiles may penetrate deep into the target, causing internal damage. This might break central contacts leading to fragmentation of an aggregate.

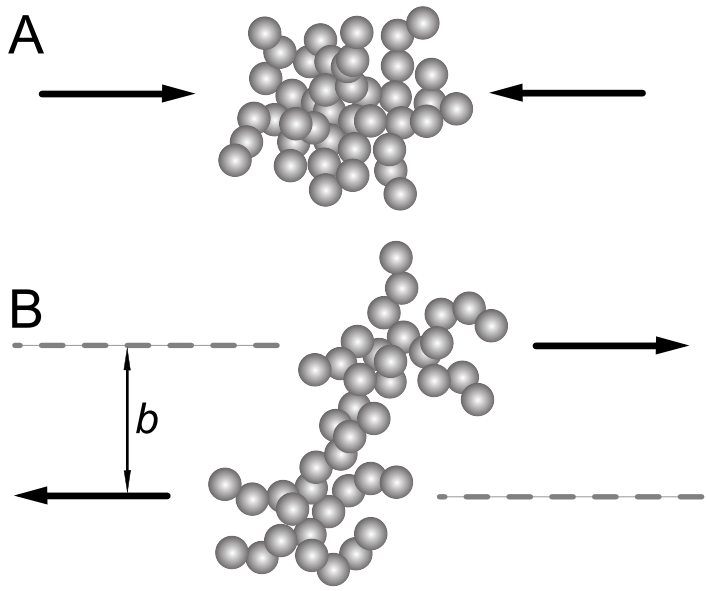

Figure 5.3 — Schematic representation of the impact parameter influence on the compression. Upper graph shows compressive, central collision, while the bottom graph presents the stretching, offset collision.

Restructuring, in the case of an impact of a small projectile, might be expected to be limited to the area of the collision. The energy sufficient to roll many monomers is also enough to break several contacts. Therefore, faster impacts are expected to result in erosion of aggregates and a limited compression (if any).

Influence of the impact parameter

Above considerations apply fully to the case of a central collision. Depending on the impact energy one may expect sticking, compression or different degrees of fragmentation. One must be, however, very careful when offset collisions are taken into account. The output of an offset impact can be dramatically different. Large offset collisions are more likely than central impacts. Thus average output of many collisions will be dominated by grazing collisions.

The difference of this type impacts is caused by a limited interaction region. Central collisions often lead to a distribution of the energy over many monomers. The grazing incident, however, involves only surface grains. Thus the kinetic energy may only affect a smaller number of monomers and contacts. Also the type of interaction plays a role. In the case of the central impact, aggregates are pushed towards each other and thus are compressed. This behavior is presented schematically in Fig. 5.3. Collisions with large impact parameter on

the other hand cause stretching of aggregates. The two colliding clusters connect, undergo some restructuring in the contact area and once the centers have passed each other, they start to pull the material out (cf. Fig. 5.3).

5.4.3 Average over the impact parameter

To allow portability of our recipe, presented in Sect. 5.6, a collision outcome is averaged over the impact parameter. This way the recipe can be easily applied to continuous models where dust growth can be studied including both the structure and the mass of fragments produced in collisions.

Since we know the products of the collisions at different offsets, we apply proper weights to that results. The weight for each impact parameter b is related to the fractional surface area of the ring with the radius b and width Δb. Thus grazing collisions get the highest weight, while the central impact has the lowest weight. The quantity Q averaged over the impact parameter is then given as

$$< Q >_b = \frac{\int_0^{b_{\max}} Q(b) 2\pi b \, \mathrm{d}b}{\pi b_{\max}^2}. \tag{5.14}$$

5.5 Results

In this section we present results of our parameter study. We discuss the influence of the initial compactness and the impact parameter in different energy regimes.

To describe results of the parameter study we choose two cases. Collisions of compact aggregates (filling factor of $\phi_\sigma = 0.251$ for smaller aggregates and $\phi_\sigma = 0.16$ for larger particles) are presented and compared with fluffy, fractal aggregates (filling factor of $\phi_\sigma = 0.155$ for small aggregates and $\phi_\sigma = 0.09$ for bigger ones). We use these two cases to illustrate the influence of compactness on the collision outcome.

The quantitative recipe in Sect. 5.6 is built using all our simulations and includes intermediate compactness aggregates as well as even more fluffy, elongated fractals.

5.5.1 Slow collisions - sticking and restructuring

Low energy collisions are highly unlikely to cause the fragmentation of aggregates. This regime includes impacts at energies from $E = 1.3 \cdot 10^{-2} E_{\mathrm{roll}}$ up to $E = 3.37 \cdot 10^{1} E_{\mathrm{roll}}$[2]. Therefore, at the lower limit no restructuring may occur, as the energy is insufficient to roll even a single contact. In the upper limit the restructuring occurs with the onset of erosion. The energy that suffice to roll many contacts is also enough to break many contacts, as the rolling energy E_{roll} is similar to the breaking energy E_{br} for our monomer size ($E_{\mathrm{br}} = 0.71 E_{\mathrm{roll}}$).

[2]Note that this is the total collision energy and not the energy per contact.

Results of these simulations at different impact parameters are presented in Fig. 5.4. Indeed, even very porous aggregates that are expected to have a

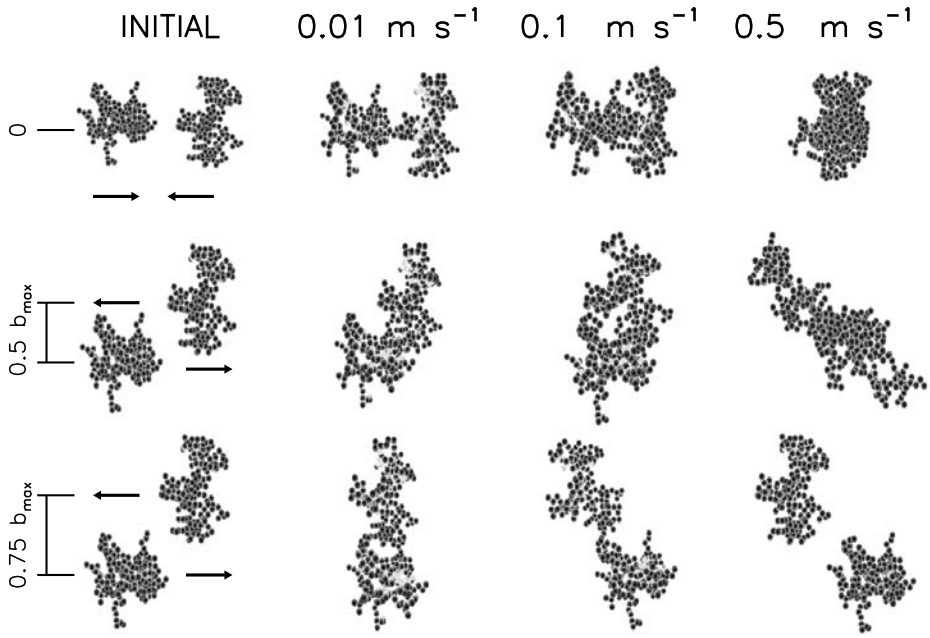

Figure 5.4 — Results of low energy impacts of fluffy aggregates of $\phi_\sigma = 0.155$. The left column shows the initial setup of the system with different impact parameters b. The following columns show results at velocities of 0.01 m/s, 0.1 m/s, and 0.5 m/s. These velocities correspond to impact energies of $1.3{\cdot}10^{-2} E_{\rm roll} = 9.2{\cdot}10^{-3} E_{\rm br}$, $1.3 E_{\rm roll} = 9.2{\cdot}10^{-1} E_{\rm br}$, and $3.37 \cdot 10^{1} E_{\rm roll} = 2.29 \cdot 10^{1} E_{\rm br}$, respectively.

weak structure are not restructured in the lowest energy collisions. The impact parameter does not play a role in these hit-and-stick events.

An increase of the impact energy leads to compression for central impacts. The third column in Fig. 5.4 shows collisions at energy $E = 1.3 E_{\rm roll}$. In this case the energy is sufficient to roll only one contact, which results in the onset of restructuring. Even though, just one contact is affected, the motion occurs somewhere inside the aggregate causing an *arm* to move. As expected, off-center collision result in tensile forces. The outcome of an impact at $b = 0.75\ b_{\rm max}$ is indeed more porous than in the case of impact parameter $b = 0$.

The effect of the impact parameter becomes stronger at higher energies. The last column in Fig. 5.4 shows strong compaction for a head-on collision and a very much elongated particle is produced in an offset impact at $b = 0.5\ b_{\rm max}$. For the larger impact parameter, the weakly distributed energy is used to break the newly established connection resulting in two large particles as before the

collision.

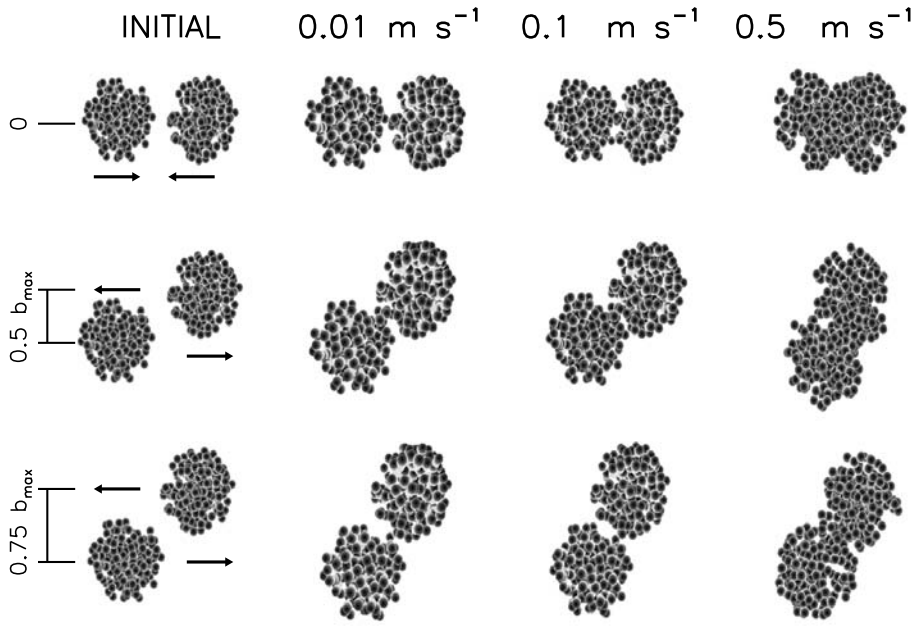

Figure 5.5 — Results of low energy impacts of compact aggregates of $\phi_\sigma = 0.251$. The left column shows the initial setup of the system with different impact parameters b. The following columns show results at velocities of 0.01 m/s, 0.1 m/s, and 0.5 m/s. These velocities correspond to impact energies of $1.3{\cdot}10^{-2}E_{\rm roll} = 9.2{\cdot}10^{-3}E_{\rm br}$, $1.3E_{\rm roll} = 9.2{\cdot}10^{-1}E_{\rm br}$, and $3.37 \cdot 10^{1}E_{\rm roll} = 2.29 \cdot 10^{1}E_{\rm br}$, respectively.

The same energies, when applied to compact aggregates, show slightly different results. Figure 5.5 presents results of collisions of compact aggregates at low energies. In the slowest impacts both head-on and offset collisions lead to sticking without restructuring. However, the increased impact energy causes rather weak, compared to fluffy aggregates, compaction. The initial aggregates are easy to recognize in the formed particle that has a dimer-like and elongated shape. The effect is even stronger in the case of grazing collisions. At higher velocities the central impacts lead to more compact aggregates, in which the identity of the involved grains is beginning to wash out, while the offset collision products still remain elongated with clear distinction of the two colliding grains.

To quantitatively describe this structural evolution, we describe it in terms of the *geometrical* filling factor ϕ_σ (cf. Eq. (5.2)). Figure 5.6 shows the filling factor of aggregates produced in central and offset collisions. The hit-and-stick impacts in Fig. 5.6A produce *dimer-like* particles. The projected surface area of these

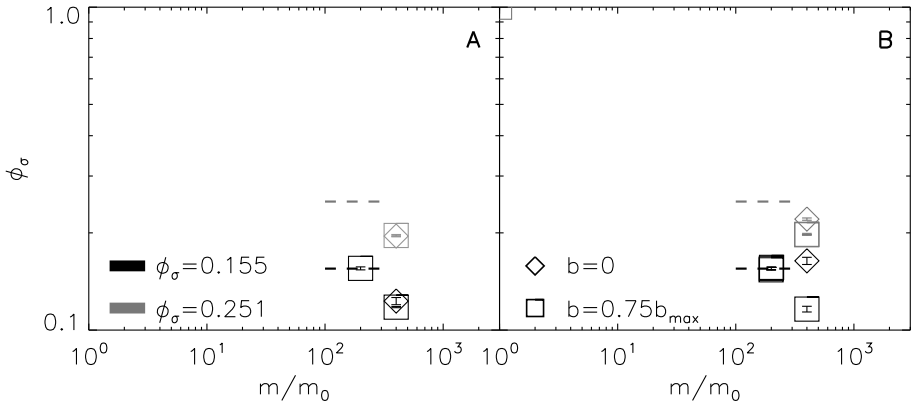

Figure 5.6 — The *geometrical* filling factor ϕ_σ of the largest fragment produced during a collision of fluffy (black symbols) and compact (grey symbols) aggregates. Diamonds indicate a head-on collision, while squares denote impact with an offset of 0.75 $b_{\max}$. Dashed lines show the initial filling factor as it was before the collision. Two panels present results of collision at different energies: impact at the energy of $E = 3.37 \cdot 10^{-1} E_{\rm roll}$ (a) and at the energy of $E = 3.37 \cdot 10^{1} E_{\rm roll}$ (b).

particles and their mass increase by approximately a factor of 2. This causes a decrease of the filling factor by a factor of about 0.7, as can be observed for both fluffy and compact aggregates in the hit-and-stick energy regime for both central and grazing impacts. The particle in Fig. 5.6A that exactly keeps the initial filling factor, is actually a missed collision.

Figure 5.6B shows results at higher impact energy. In this case restructuring takes place, which is indicated by a significant difference between head-on and offset collisions. As discussed before, this difference is small for compact aggregates. Porous particles, on the other hand, suffer a true compression when they collide head-on. The filling factor of these aggregates increases above the initial value of $\phi_\sigma = 0.155$. The products of collision at large impact parameter, however, move to even lower filling factors.

The effect of the mass ratio on the structural change of aggregates at low energies is presented in Fig. 5.7a. Single monomers at 0.5 m/s have an energy below $E_{\rm br}$ and thus are in the hit-and-stick regime. Larger aggregates at this velocity have sufficient energy to cause some restructuring. Compact aggregates are very weakly affected and their filling factor remains unchanged. Fluffy particles are only slightly compressed, and their filling factor increases only by about 1%. Collisions with mass ratio of 0.1 lead to a similar result. A higher impact energy causes both stronger compaction and the onset of erosion (see Fig. 5.7b). Compact aggregates are slightly compressed by collisions with mass ratio above 0.1. In the case of the smallest mass ratio ($m_1/m_2 = 10^{-3}$), the impact energy is insufficient to roll even a single contact ($E = 0.76\ E_{\rm roll}$).

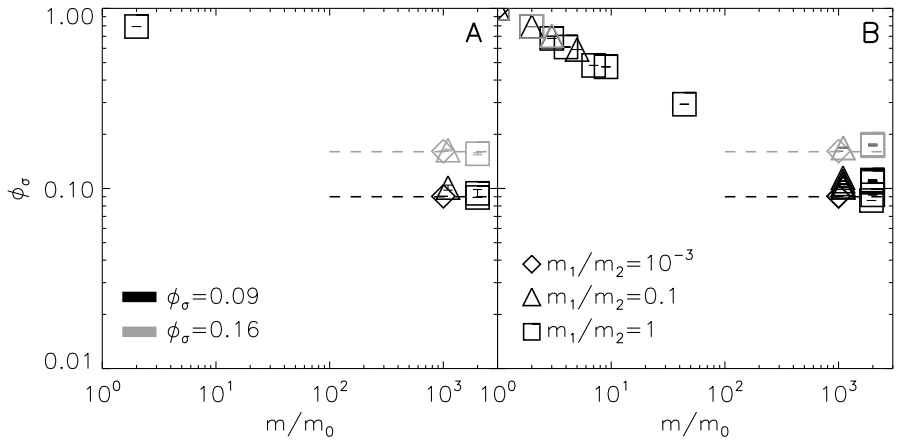

Figure 5.7 — The *geometrical* filling factor $\phi_\sigma$of the largest fragment produced during a collision of fluffy (black symbols) and compact (grey symbols) aggregates made of 1000 monomers with different size particles. Diamonds indicate single monomer impactors, triangles denote projectiles made of 100 monomers, and squares represent particles made of also 1000 monomers. Left panel (a) corresponds to slow impacts at velocity of 0.5 m/s, while the right panel (b) at velocities of 0.75 m/s. All collisions are head-on.

5.5.2 Intermediate speed collisions - erosion

Here we present intermediate energy collisions that result in a strong compaction of aggregates. We chose this energy regime to extend from the onset of erosion at energy of about $E \approx 0.1 N E_{\rm br}$ up to the onset of shattering ($E \approx N E_{\rm br}$).

In the case of silicates, these limits correspond, to $E \approx 0.15 N E_{\rm roll}$ and $E \approx 1.5 N E_{\rm roll}$, respectively. Therefore, we expect the maximum compression to occur somewhere in this regime.

Figure 5.8 shows results of collisions of fluffy particles at different energies and impact parameters. Central collisions cause erosion, which becomes stronger at higher velocities. The compaction is also noticeable, but only at lower velocities. Interestingly, larger energies are not only sufficient to strongly compress particles, but the excess of the energy continues to restructure the aggregate, which results in flattening and decompression of particles. This decompression is "formal" in the sense that ϕ_σ decreases due to the pancake-like shape of the resulting aggregate, not due to changes to true internal density. The offset collision on the other hand, causes very strong elongation of aggregates until the energy suffice to break most of the contacts ($E = 0.92\ N\ E_{\rm br}$). At that point the strong erosion sets in, removing part of the mass. The grazing collision however produces two collision remnants. In this case a weak erosion is observed only in collision with the highest energy.

Collisions of the compact aggregates are presented in Fig. 5.9. The erosion

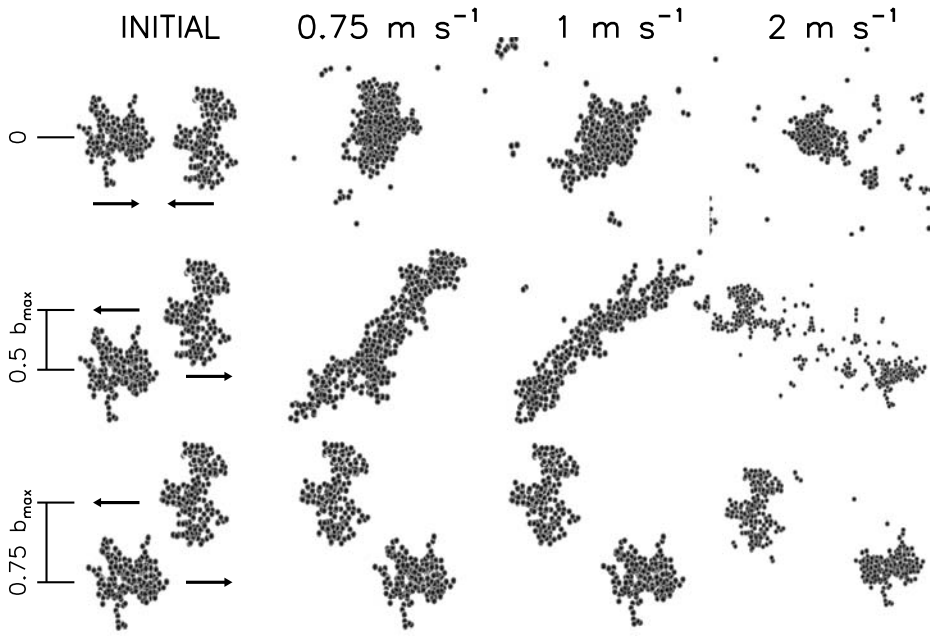

Figure 5.8 — Results of the intermediate energy impacts of fluffy aggregates of ϕ_σ = 0.155. The left column shows the initial setup of the system with different impact parameters b. The following columns show results at velocities of 0.75 m/s, 1.0 m/s, and 2.0 m/s. These velocities correspond to impact energies of $1.9 \cdot 10^{-1} NE_{\rm roll} = 1.3 \cdot 10^{-1} NE_{\rm br}$, $3.4 \cdot 10^{-1} NE_{\rm roll} = 2.3 \cdot 10^{-1} NE_{\rm br}$, and $1.35 NE_{\rm roll} = 9.2 \cdot 10^{-1} NE_{\rm br}$, respectively.

process is much weaker than in the case of the fluffy aggregates. The impacting particles are compacted more strongly, such that at 1 m s^{-1} the dimer-like shape of the produced aggregate changes to approximately spherical shape. At 2 m s^{-1} (this correspond to energy of $E = 0.91 NE_{\rm br}$), however, the collision product is flattened into a pancake-like structure, similarly to fluffy particles.

Offset collisions of the compact particles still produce *dimer-like* aggregates, and show stronger resistance to stretching compared to fluffy particles. At the highest energy in this regime, off-center impacts result in two aggregates of approximately equal mass. The impact parameter $b = 0.5\ b_{\rm max}$ causes stronger restructuring that can, in the presence of tensile forces, result in the formation of elongated *arms* on the surface of aggregates (see last column in Fig. 5.9).

Quantitatively, these results are presented in Fig. 5.10. The filling factor of the produced particles increases in head-on collisions. Fluffy aggregates are compressed significantly reaching packing densities well above the initial value. offset collisions result in a few cases in a strong *decompression*. Some aggregates, however, detach producing two particles with the filling factor similar to

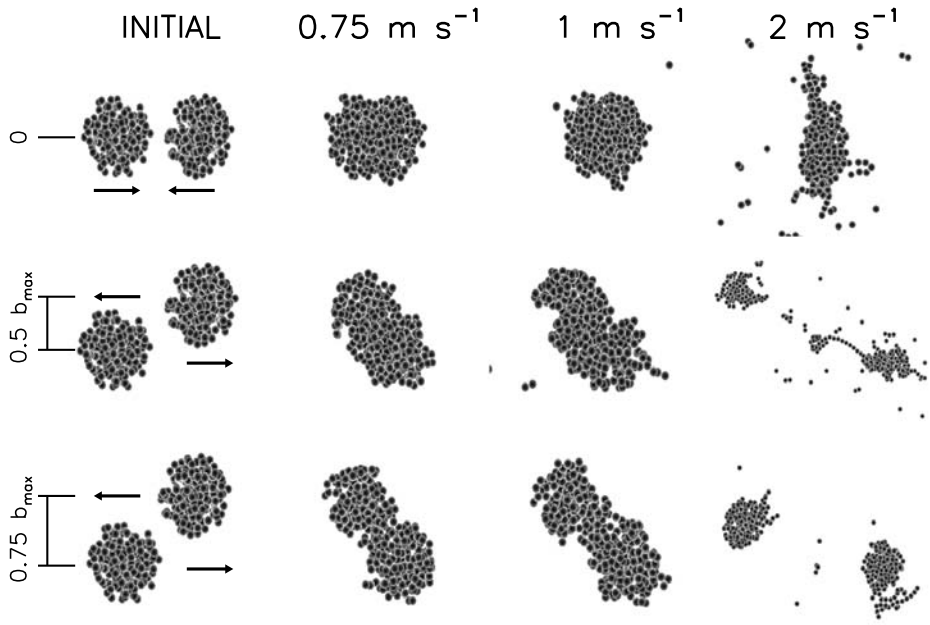

Figure 5.9 — Results of the intermediate energy impacts of compact aggregates of ϕ_σ = 0.251. The left column shows the initial setup of the system with different impact parameters b. The following columns show results at velocities of 0.75 m/s, 1.0 m/s, and 2.0 m/s. These velocities correspond to impact energies of $1.9 \cdot 10^{-1} NE_{\text{roll}} = 1.3 \cdot 10^{-1} NE_{\text{br}}$, $3.4 \cdot 10^{-1} NE_{\text{roll}} = 2.3 \cdot 10^{-1} NE_{\text{br}}$, and $1.35 NE_{\text{roll}} = 9.2 \cdot 10^{-1} NE_{\text{br}}$, respectively.

the initial value. An increase of the impact energy results in strong erosion for fluffy particles (see Fig. 5.10B). However, small fragments are produced mostly by central collision. In the case of grazing impact the erosion is limited and two big fragments of initial compactness are the outcome.

Compact aggregates are more difficult to compress. Their filling factor ϕ_σ reaches at most the initial value. Higher energies lead to a lower filling factor reaching values below 20%.

The mas ratio effect in this energy regime is not much different from the low energies. Aggregates are weakly affected by small projectiles in terms of the filling factor (see Fig. 5.7). The surface added or removed may be noticeable only in the case of multiple, successive impacts. However, these are not subject of this parameter study.

The intermediate energy regime leads to the loss of small fragments. Since only a small fraction of the mass is lost (less that a half of the total mass of both impacting aggregates), we classify this outcome as *erosion*. The collision can be quantified in terms of the largest collision remnant. Figure 5.11 shows this

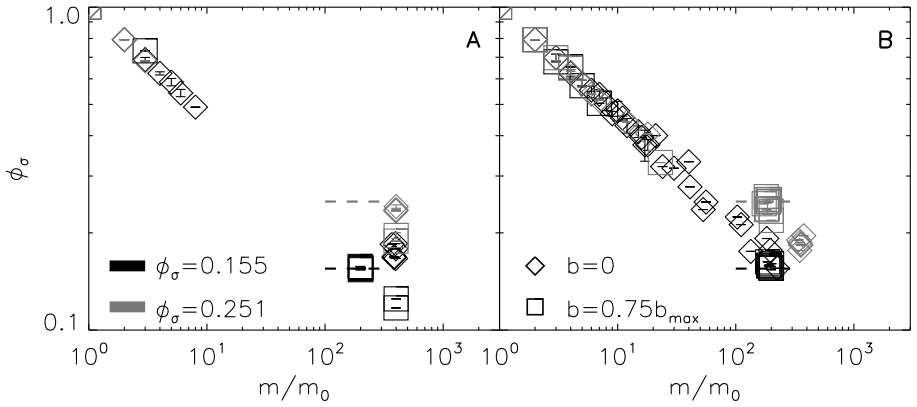

Figure 5.10 — The *geometrical* filling factor ϕ_σ of the largest fragment produced during a collision of fluffy (black symbols) and compact (grey symbols) aggregates. Diamonds indicate a head-on collision, while squares denote impact with an offset of $0.75b_{\max}$. Dashed lines show the initial filling factor as it was before the collision. Two panels present results of collision at different energies: impact at the energy of $E = 1.9 \cdot 10^{-1} NE_{\rm roll}$ (a) and at the energy of $E = 1.35NE_{\rm roll}$ (b).

quantity as a function of impact energy for both fluffy and compact aggregates. At low impact energies (the hit-and-stick regime), fluffy aggregates show that the largest fragments has only about 90% of the total mass. This is the effect of collisions that miss or feature very limited interaction leaving the original aggregates mostly intact.

The lowest velocities indeed lead to perfect sticking and locking of the total mass in one big aggregate. The decrease of the mass of the largest fragment marks the onset of the erosion regime. This process begins at very similar energies for both compact and fluffy aggregates. However, it is much stronger for porous particles. At energy of $E = 0.5NE_{\rm br}$ fluffy aggregates loss about half of the total mass, while compact particles loss only about 10% to 30% depending on impact parameter. The picture changes only at very high energies, when fragmentation takes over. This, however, we discuss in the next section.

A more complete picture is presented by a distribution of fragment masses. This is illustrated for central impacts in Fig. 5.12. Collisions at intermediate speeds erode aggregates and produce a number of the small fragments. Two components can be separated in these distributions. The small fragments component and the large particle component.

The distribution of small particles is a power-law

$$f(m/m_0)(m/m_0)^2 \propto m^q, \tag{5.15}$$

with the slope q depending on several parameters, including the internal structure of aggregates and the impact energy. Initially too few small particles are

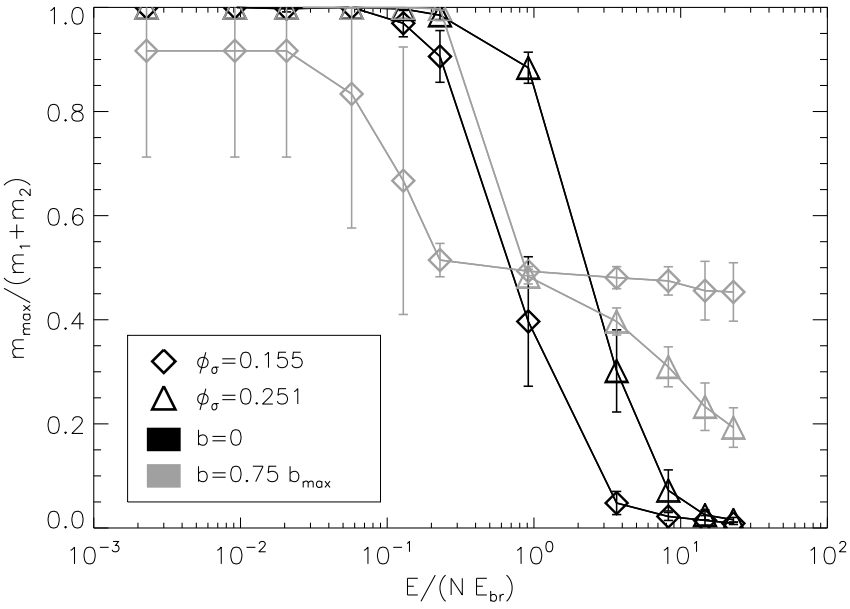

Figure 5.11 — The mass of the largest collision remnant for central and offset collisions as a function of the impact energy. Diamonds correspond to compact aggregates, while triangles correspond to fluffy particles. Error bars indicate standard deviation and each point represents a mean value for 6 individual simulations (see Sect. 5.3).

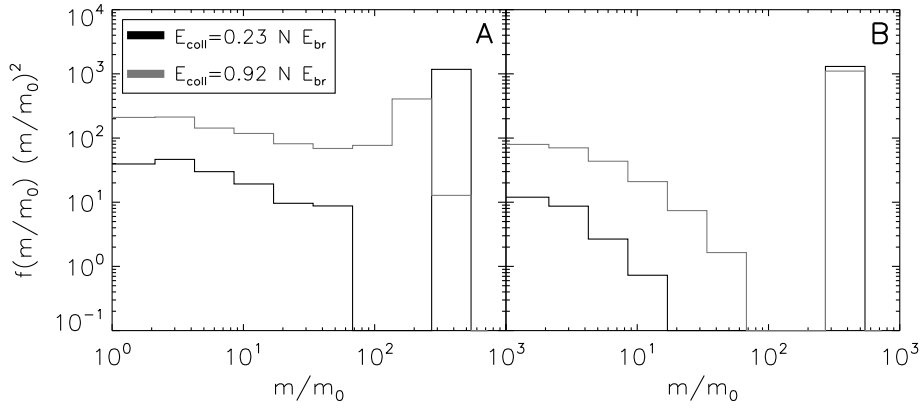

Figure 5.12 — Mass distribution as resulted from head-on collisions of (a) fluffy (ϕ_σ = 0.155) and (b) compact (ϕ_σ = 0.251) aggregates at two intermediate impact energies.

produced and the power-law cannot be determined. In such a case we assume that the distribution is flat with the slope $q = 0$, meaning equal mass per logarithmic mass interval. As the erosion progresses with increasing impact energy, the fitted slope remains relatively low. Small particles slightly dominate the mass within this power-law distribution, since the fitted slope is about $q \approx -0.3$ in the case of fluffy aggregates (Fig. 5.12a) and about $q \approx -1.2$ for compact aggregates (Fig. 5.12b).

This behavior is similar for offset collisions (see Fig. 5.13). Although, erosion is much weaker, the two components are clearly visible. The slope of small

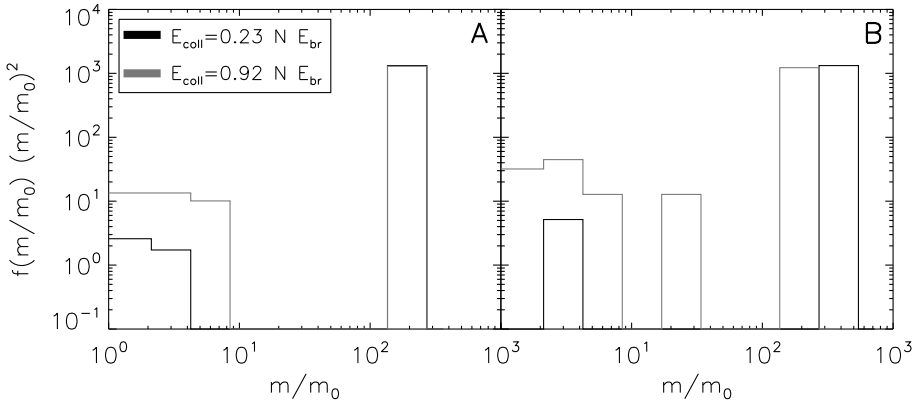

Figure 5.13 — Mass distribution as resulted from off-center ($b = 0.75\, b_{\max}$) collisions of (a) fluffy ($\phi_\sigma = 0.155$) and (b) compact ($\phi_\sigma = 0.251$) aggregates at two intermediate impact energies.

fragments component, however, cannot be fitted due to a limited data. Fluffy aggregates when colliding at the energy of $E = 0.23 N E_{\rm br}$ and higher produce two large fragments that contribute to the big particles component and a few small particles. Compact aggregates still grow at the energy of $E = 0.23 N E_{\rm br}$ producing only one large fragment and a cloud of small particles.

Although intermediate energies are required to erode particles in collisions of equal mass aggregates, this is not the case for impacts with large mass ratios. Energy is localized in a small region leading to erosion. Figure 5.14 shows the effect of the mass ratio on the mass distribution of fragments. The top panels (Fig. 5.14a & Fig. 5.14b) illustrate the mass distribution for impacts of a monomer onto an aggregate composed of 1000 grains. In these cases, the energy is sufficient to break only a small number of contacts[3] and results in erosion. However, in some collisions a monomer penetrates deeper into a fluffy target, breaking only a few contacts holding large parts of an aggregate together. Large

[3]Note that in Fig. 5.14a & Fig. 5.14b the energy is normalized to the reduced number of monomers $N_\mu = \frac{N_1 N_2}{N_1 + N_2}$. Therefore the energy per contact is a factor of 10^3 lower.

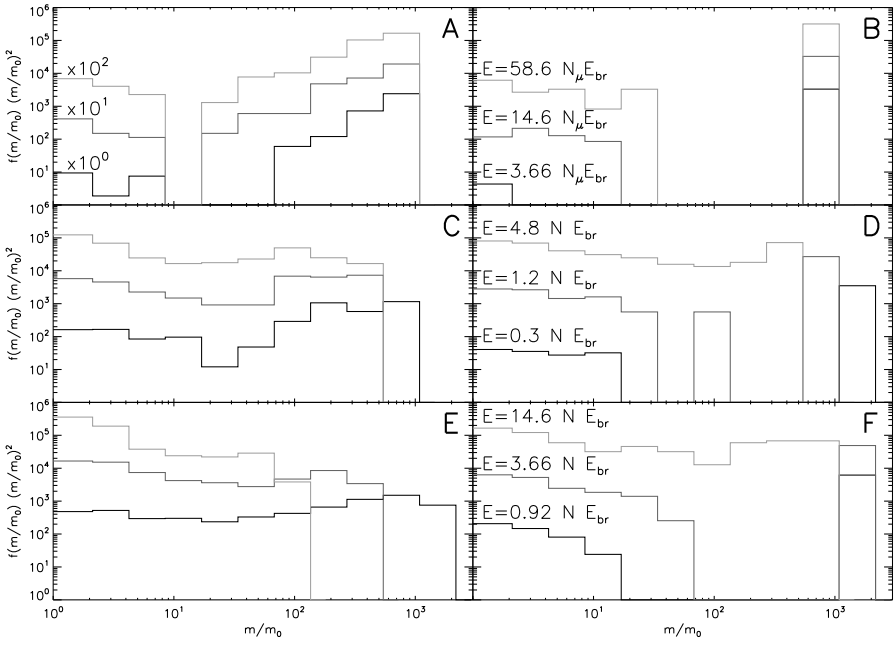

Figure 5.14 — Mass distribution as resulted from central collisions between aggregates of different mass ratios and at different energies. Left panels show collisions of fluffy aggregates with the filling factor of $\phi_\sigma = 0.09$, while the right panels show impacts of compact particles with $\phi_\sigma = 0.16$. Different mass ratios are presented in an increasing order from top to bottom: a&b – mass ratio $m_1/m_2 = 10^{-3}$; c&d – mass ratio $m_1/m_2 = 0.1$; e&f – mass ratio $m_1/m_2 = 1$. The energy in top panels is normalized to the reduced number of monomers $N_\mu = N_1 N_2/(N_1 + N_2)$ and not to a total number of particles (or contacts) N like in other panels.

fragments result, filling the gap between the distribution of small fragments and the large fragment peak. Compact particles, on the other hand are more difficult to penetrate, which results clearly separate components. The slope of the mass distributions is again in the range of $q \approx -0.3$ to $q \approx -1$.

In the case of larger mass ratio of $m_1/m_2 = 0.1$ (Fig. 5.14c & Fig. 5.14d), the increasing energy causes the erosion to increase. Fluffy aggregates start to be shattered at energies sufficient to break all contacts in both aggregates ($E = N\,E_{\rm br}$). The power-law component steepens ($q \approx -0.7$) indicating onset of the fragmentation. In the case of compact particles, the slope of the distribution of small fragment masses still remains relatively shallow ($q \sim -0.3$). At high energies more than half of the mass is removed meaning that shattering occurs.

Collision of equal mass aggregates (Fig. 5.14e & Fig. 5.14f) also result in a strong erosion if the impact energy remains below $E = N\,E_{\rm br}$. Higher energies lead to fragmentation and even shattering. This takes us to the fragmentation

regime.

5.5.3 Fast collisions - fragmentation

Fast impacts provide a sufficient amount energy to break all contacts in an aggregate. Therefore, the fragmentation is severe and may completely shatter colliding particles. Although, this is true in the case of the central collision, the effect is significantly decreased for the offset impacts. The higher the impact parameter, the less destruction is caused. The grazing collisions even at the highest velocities cause only erosion of the aggregates. The sample images for the fluffy aggregates are shown in Fig. 5.15. Indeed the fragmentation gains in strength

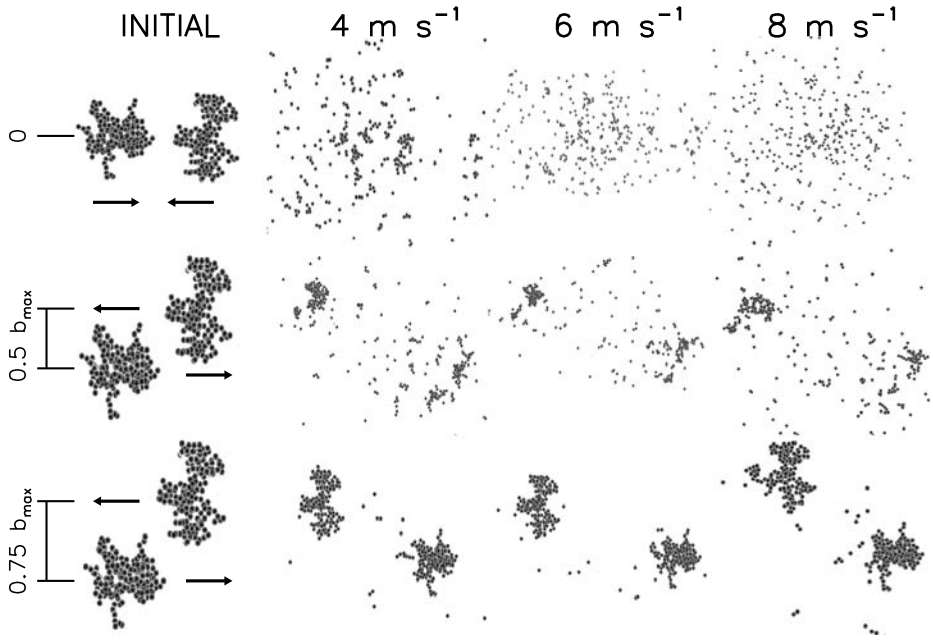

Figure 5.15 — Results of the high energy impacts of fluffy aggregates of $\phi_\sigma = 0.155$. The left column shows the initial setup of the system with different impact parameters b. The following columns show results at velocities of 4 m/s, 6 m/s, and 8 m/s. These velocities correspond to impact energies of $5.4NE_{\rm roll} = 3.66NE_{\rm br}$, $1.21 \cdot 10^1 NE_{\rm roll} = 8.2NE_{\rm br}$, and $2.16 \cdot 10^1 NE_{\rm roll} = 1.46 \cdot 10^1 NE_{\rm br}$, respectively.

to become catastrophic as the velocity increases. Note, however, that in grazing collisions even the highest energies cause only erosion.

The central collisions of the compact aggregates lead to a similar result (see Fig. 5.16). The fragmentation becomes stronger with increasing impact energy for the central collisions. The impact parameter, however, has weaker influence

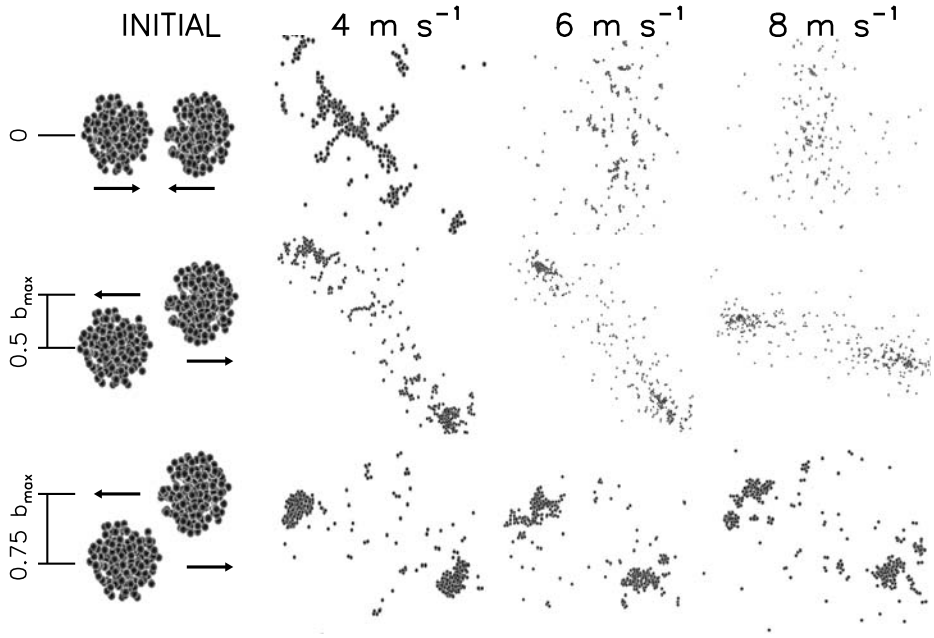

Figure 5.16 — Results of the high energy impacts of compact aggregates of $\phi_\sigma = 0.251$. The left column shows the initial setup of the system with different impact parameters b. The following columns show results at velocities of 4 m/s, 6 m/s, and 8 m/s. These velocities correspond to impact energies of $5.4NE_{\rm roll} = 3.66NE_{\rm br}$, $1.21 \cdot 10^1 NE_{\rm roll} = 8.2NE_{\rm br}$, and $2.16 \cdot 10^1 NE_{\rm roll} = 1.46 \cdot 10^1 NE_{\rm br}$, respectively.

on the outcome in this case than for fluffy particles. Even grazing collisions lead to nearly complete disruption.

The effect of offset impacts and energies is even clearer in Fig. 5.17 and Fig. 5.18, where we show the fragment mass distribution. The head-on collision at energy of $E = 3.66NE_{\rm br}$ completely shatters fluffy aggregates with the largest fragment having only about 15% of the total mass. The large fragment component disappears altogether, shifting the entire mass into the steep power-law with the slope $q \approx -1$. Further increase of the energy results in heavier damage and steeper slope. At the energy of $E = 14.6NE_{\rm br}$ the slope reaches $q \approx -2.5$.

Although a similar trend is observed for compact particles, equal degree of destruction occurs at higher energies (see Fig. 5.17b). A head-on impact of compact particles at the energy of $E = 3.66NE_{\rm br}$ still resembles the erosion case. The large fragments component is still present and contains a significant fraction of the mass. The slope of the power-law remains shallow at $q \approx -0.3$. An increase of the energy to $E = 14.6NE_{\rm br}$ shatters the aggregates, leaving only the power-law component with a steeper slope of about $q \approx -2$.

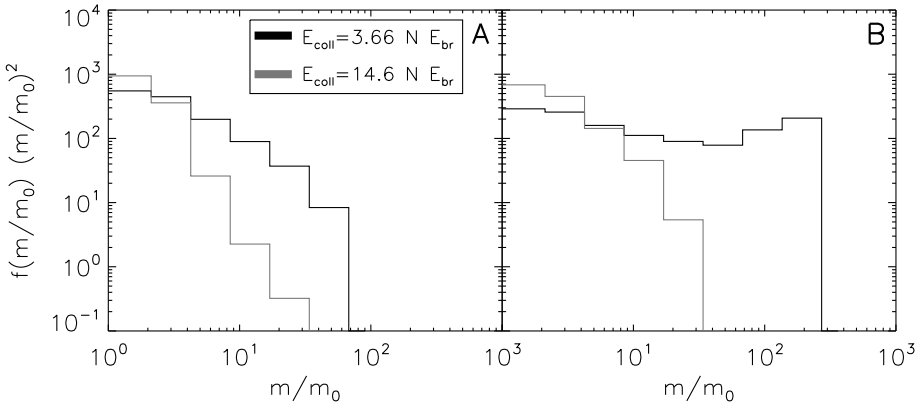

Figure 5.17 — Mass distribution as resulted from head-on collisions of a – fluffy (ϕ_σ = 0.155) and b – compact (ϕ_σ = 0.251) aggregates at two high impact energies.

Off-center collisions (see Fig. 5.18) are characterized by distributions that

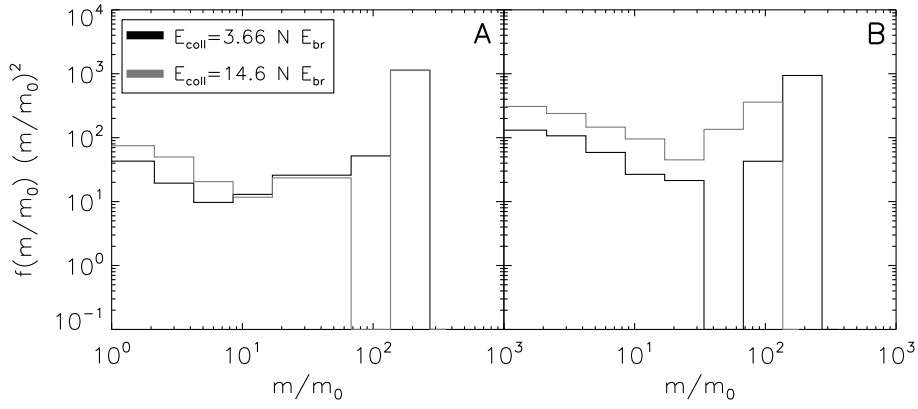

Figure 5.18 — Mass distribution as resulted from off-center collisions of a – fluffy (ϕ_σ = 0.155) and b – compact (ϕ_σ = 0.251) aggregates at two high impact energies.

resemble the erosion case. A highly pronounced large fragment component coexists with a power-law distribution of small fragments. The similarity with the erosion case is also visible in the energy independent slope. It remains constant at $q \approx -1$ for fluffy aggregates and $q \approx -0.6$ for compact particles.

The effect of the energy on the slope of the power-law distribution is presented in Fig. 5.19. The left panel (A) shows the results for fluffy aggregates. Initially shallow and constant slopes begin to steepen once the impact energy increases above $E = NE_{\rm br}$. This behavior is similar for aggregates of different

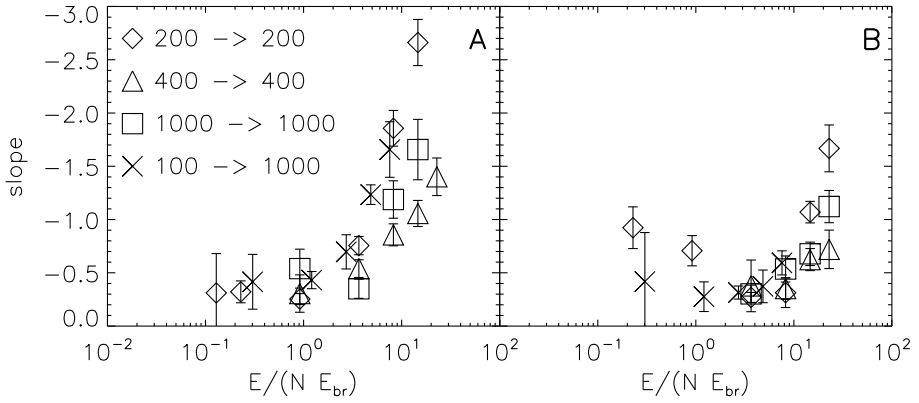

Figure 5.19 — Slopes of the power-law size distribution of small fragments as a function of impact energy. Different symbols correspond to different mass of colliding aggregates. Left panel (a) corresponds to fluffy aggregates ($\phi_\sigma = 0.09 \ldots 0.155$), while the right panel (b) shows result of collisions between compact aggregates ($\phi_\sigma = 0.16 \ldots 0.251$).

mass or mass ratio. Note that for very weak erosion the slope of the power-law cannot be determined and a value of $q = 0$ is assumed. The shattering becomes catastrophic when the energy increases by an order of magnitude. The slope steepens beyond $q = -1$, meaning that small particles significantly dominate the mass spectrum. For small aggregates the distribution may be as steep as $q = -2.5$.

Compact particles behave in a similar manner (see Fig. 5.19B). In this case, however, the steepening occurs at slightly higher energies of about $E = 5NE_{\rm br}$. Moreover the steepening is limited in the explored energy range, and reaches values of $q = -1.7$. In this case low energies also result in shallow slopes of the distribution and are assumed to be $q = 0$, when the data was too scarce to make a fit.

The structural evolution of aggregates in this high energy regime is mostly determined by the filling factor of small fragments. Interestingly, it tightly follows a power-law function of particle mass with a slope of -0.33. This is clearly illustrated in Fig. 5.10B, and Fig. 5.20. Regardless of the initial compactness, impact energy or impact parameter, small fragments are very well described by a simple relation. Large particles can survive only grazing collisions, which lead to very short and localized interaction. Therefore, in grazing collisions of fluffy aggregates, the structure remains unchanged. In the case of compact particles, however, the interaction involves more grains at a given impact parameter, leading to erosion and restructuring.

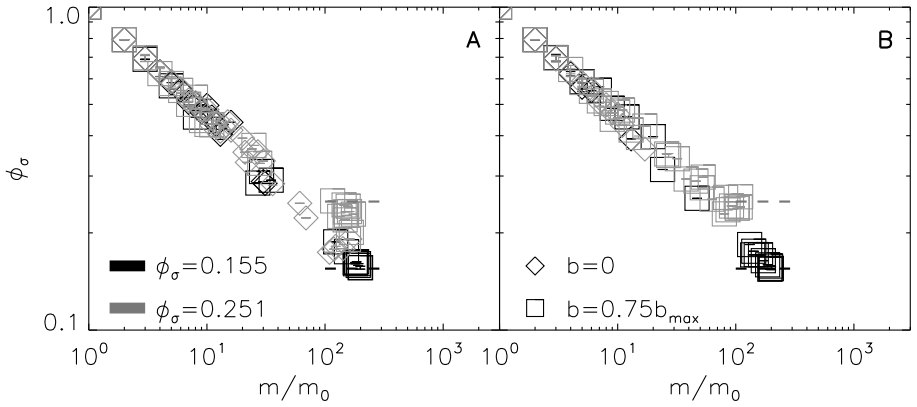

Figure 5.20 — The *geometrical* filling factor ϕ_σ of the largest fragment produced during a collision of fluffy (black symbols) and compact (grey symbols) aggregates. Diamonds indicate a head-on collision, while squares denote impact with an offset of $0.75b_{\max}$. Dashed lines show the initial filling factor as it was before the collision. Two panels present results of collision at different energies: impact at the energy of $E = 5.4NE_{\rm roll}$ (a) and at the energy of $E = 2.16 \cdot 10^1 NE_{\rm roll}$ (b).

5.6 The Recipe

In this section we put together the information regarding the collisional output in a form of a quantitative recipe. We provide the recipe in a form of tables that contain parameters needed to reconstruct appropriate distributions. Since the recipe is provided as discrete parameters, the intermediate cases should be interpolated. Our recipe describes two limiting cases separately. Equal mass collisions affect aggregates globally. Therefore we refer to this sub-recipe as the global recipe. On the other hand we have large mass ratio impacts that result in a localized changes. This sub-recipe is referred to as the local recipe. In this case of large mass ratio collisions, we use impacts of monomers onto aggregates composed of 1000 grains. In this case central collisions are used also for the non missed offset impacts because the effects are extremely similar. This assumes that the geometry of the impact of small projectile onto a larger target depends on a local surface. Thus central and offset collisions should be indistinguishable. The only necessary correction is to exclude missed collisions that are more likely at larger impact parameters. The distinction between the two sub-recipes is described later in Sect. 5.6.4.

5.6.1 Hit and stick recipe

Although, our simulations include the hit-and-stick energy regime, this growth mechanism strongly depends on the mass ratio and should be treated separately.

Table 5.4 — Quantities provided by the recipe to reproduce the mass distribution.

symbol	description
q	The slope of the power-law component.
M_r	ratio of the mass in the power-law component to the mass in the Gaussian component.
σ_G	Width of the Gaussian component.
M_G	Mean mass of the Gaussian component.

The hit-and-stick growth is of little importance, when only an insignificant mass is added before any restructuring occurs. Otherwise, an analytical prescription may be applied as in Ossenkopf (1993); Ormel et al. (2007, 2008b); Paszun et al. (2008).

5.6.2 Distribution of fragment mass

The simulation results have shown that collisions produce two components. The first component - the power-law of small fragments - is produced in high energy, head-on impacts resulting in erosion and fragmentation. The second component - the distribution of the largest fragments - is formed during low energy impact, and by grazing collisions at all energies. We model this component using a Gaussian. It is thus expected that the power-law steepens as the impact energy increases and that the peak of the Gaussian moves to smaller masses. This is caused by the erosion and the fragmentation, that result in a decrease of the mass of the largest fragment and an increase of the mass in the power-law component.

The total set of parameters needed to reproduce such a distribution is presented in Tab. 5.4. The power-law component is determined by fitting a power-law to the first part of the distribution, which contains small fragments. That fitted power-law is then subtracted from the distribution. The power-law slope and mass ratio of the two components is known at this point. The remaining part of the distribution is used to determine the last 2 quantities, namely the mean and the width of the Gaussian component. The mean mass M_G is simply the mass weighted mean mass of fragments in the Gaussian component

$$M_\mathrm{G} = \frac{\int_{\log m_0}^{\log(m_1+m_2)} m f(m/m_0)(m/m_0)^2 \mathrm{d}\log m}{\int_{\log m_0}^{\log(m_1+m_2)} f(m/m_0)(m/m_0)^2 \mathrm{d}\log m}. \tag{5.16}$$

The width of the Gaussian is chosen to obey two constraints:

1. the Gaussian should have a sharp cut-off at masses larger than the total mass of colliding aggregates.
2. the power-law component must dominate the low mass part of the distribution.

To present the representative fragment distribution we average the mass spectrum over the impact parameter (see Sect. 5.4.3). Some impact parameter averaged distributions are shown in Fig. 5.21. The panels show the evolution of

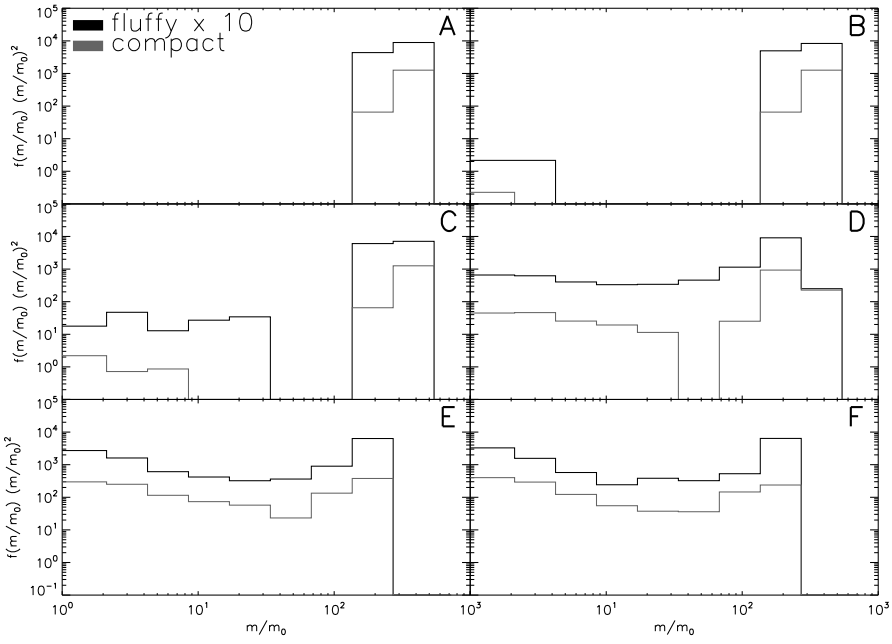

Figure 5.21 — Distributions averaged over the impact parameter. Results for fluffy and compact aggregates at energies $E = 5.7 \cdot 10^{-4} NE_{\rm br}$ (a), $E = 5.7 \cdot 10^{-2} NE_{\rm br}$ (b), $E = 0.13 NE_{\rm br}$ (c), $E = 0.92 NE_{\rm br}$ (d), $E = 8.2 NE_{\rm br}$ (e), and $E = 14.6 NE_{\rm br}$ (f).

mass spectrum for both compact and fluffy aggregates. At low energies growth dominates. Grazing collisions, however, contribute to a lower mass bin causing a slight decrease of the mean mass. An increase of the energy leads to the onset of erosion. Small fragments appear with a very flat slope of the power-law distribution. Further increase of the energy enhances the erosion. The component of small fragments grows and begins to slightly steepen the slope. Eventually growth changes into fragmentation. The large fragments component, however, remains in the distribution caused by the grazing collisions. The impact parameter average reduces both the effect of fragmentation and differences between fluffy and compact particles.

5.6.3 Compactness evolution

The filling factor ϕ_σ, similarly to mass spectrum, shows different behavior between central and offset collisions. The effect of impact parameter averaging

is presented in Fig. 5.22. Compact aggregates are decompressed. At higher

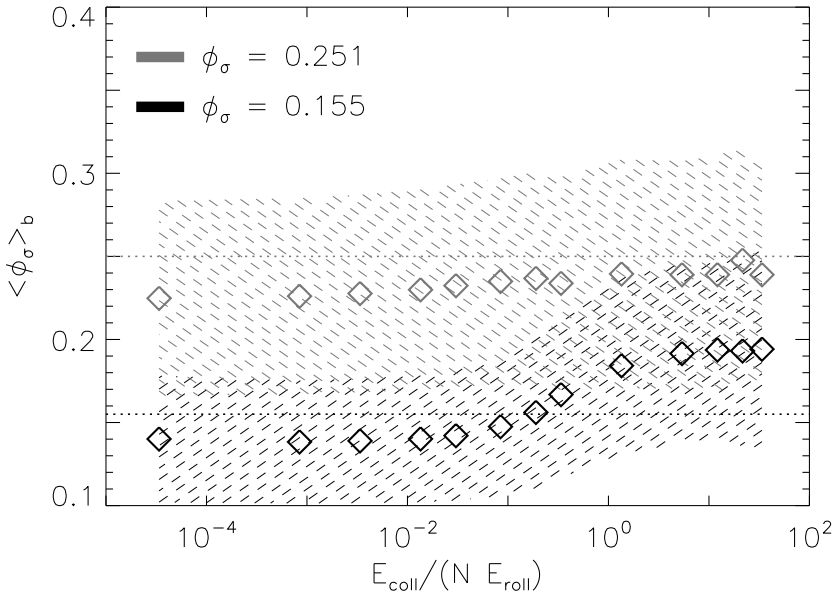

Figure 5.22 — The filling factor ϕ_σ averaged over the impact parameter vs the collision energy scaled with the number of monomers N and in units of the rolling energy $E_{\rm roll}$. The dashed areas correspond to the spread around the mean value. The dotted lines indicate the initial value of the filling factor for the colliding particles.

energies of about $E = NE_{\rm roll}$ aggregates undergo compression that mostly compensates the offset collisions and the *dimer-like* structure discussed in Sect. 5.5.

Fluffy aggregates also increase porosity in low energy collisions. The increasing energy, however, causes both a decrease of the mass of the largest fragment and compaction of the aggregates. The grazing collisions at a high energy produce aggregates with weakly changed structure. Therefore the structural change is dominated by compressing head-on impacts. A further increase of the collision energy results in a stronger compression. The maximum filling factor of about $\phi_\sigma \approx 0.19$ is reached at $E = NE_{\rm roll}$. A further increase of the energy does not affect the porosity. Particles are completely disrupted and the filling factor is dominated by small, fluffy fragments (see Fig. 5.20).

Small fragments produced by erosion or fragmentation are easily described by a single power-law. Regardless of initial porosity of the impact energy, small particles have the filling factor given by

$$\phi_\sigma = (m/m_0)^{-0.33}. \tag{5.17}$$

5.6.4 Format

Our recipe provides parameters required to reconstruct mass distribution averaged over impact parameter. The distribution of the fragment masses is given by $F(m)\,\mathrm{d}\log m = f(m)\,m^2\,\mathrm{d}\log m$, where $f(m)\,\mathrm{d}m$ provides the number of particles of mass m in mass interval between m and $m + \mathrm{d}m$. Thus the functional form of our recipe consists of the two components and is given by

$$F(m) = \xi_1 m^q + \frac{\xi_2}{\sqrt{2\pi}\sigma_\mathrm{G}} \exp \frac{-(m - M_\mathrm{G})}{2\sigma_\mathrm{G}^2}, \tag{5.18}$$

where ξ_1 and ξ_2 are the normalization constants of the power-law component and the Gaussian, respectively. Please note that they are not provided since the distribution should be re-normalized in order to conserve the mass. Instead we give ratio of the power-law component to the Gaussian component, which should be used to determine the mass and normalization constant in each component. The power-law component extends from a monomer mass to a quarter of the total mass.

Our recipe is provided in tabulated form. The parameters required to reproduce the collisional outcome may be interpolated linearly. Our parameter space is covered very well and spans from very fluffy aggregates of fractal dimension $D_\mathrm{f} = 1.5$ through fluffy fractal ($D_\mathrm{f} = 2.0$) and non fractal PCA aggregates to very compact particles of $\phi_\sigma = 0.251$. The energy space is also well sampled. Our recipe is based on simulations from hit-and-stick regime up to a catastrophic destruction.

The difference between the local and the global sub-recipes is due to mass ratio effect. However, small projectiles, when carrying sufficient energy (i.e.,impacting with very high speeds), may also shatter an entire target aggregate. Therefore the global recipe is applicable not only at mass ratio close to unity, but also when the energy is sufficient to globally affect an aggregate. Figure 5.23 presents a scheme of the algorithm used to distinguish between the local and the global recipes. When a collision of aggregates characterized by their masses m_i, filling factors ϕ_i, and some material properties, occurs at a given impact energy, one must check whether the collision is in the recipe domain (restructuring or fragmentation) or in a hit-and-stick regime. The test checks whether the energy is sufficient to cause any restructuring. If the condition $E_\mathrm{coll} < 5E_\mathrm{roll}$ is satisfied, the hit-and-stick mechanism is applied (for details see Ormel et al. (2007), Ormel et al. (2008b)). Otherwise, a second check is performed. If any of the two following conditions is true, the global recipe is applied:

$$\frac{m_1}{m_2} > 0.1, \tag{5.19}$$

or

$$E > 5NE_\mathrm{br}. \tag{5.20}$$

If none of the above is true, the local recipe must be used.

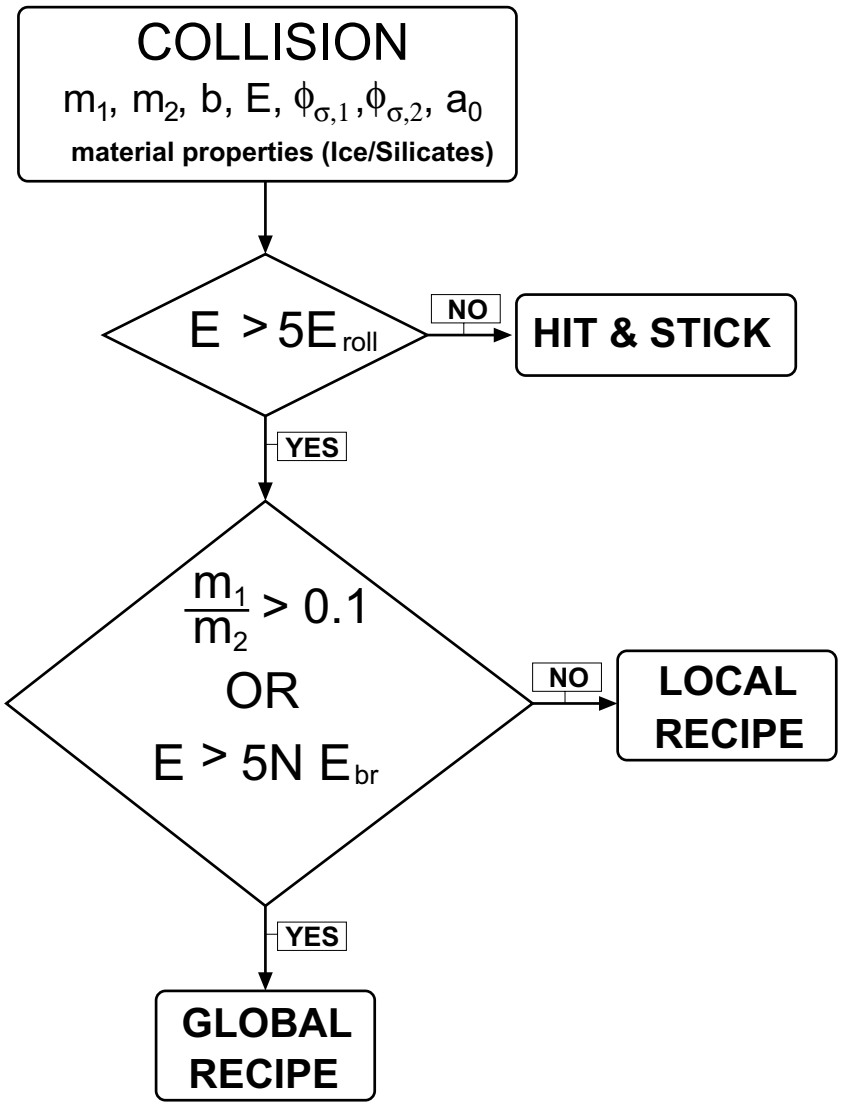

Figure 5.23 — Scheme of an algorithm that should be used to distinguish between the global and the local recipes.

The recipe provides a description of the outcome of a collision between aggregates of the same filling factor. To describe collision of aggregates with different compactness, a mass weighted average filling factor must be determined

$$< \phi_\sigma >_m = \frac{\sum_i \phi_{\sigma,i} m_i}{\sum_i m_i}. \tag{5.21}$$

Therefore the filling factor that should be used is dominated by that of the more massive aggregate. In particular the outcome of a collision between particles of different mass depends very much on the porosity of the target aggregates and how deep it can be penetrated. Collisions of equal mass particles on the other hand are not dominated by one species. Therefore the contribution from both aggregates should be about equal. The compression or decompression is expected to be weaker than for fluffy particles, as compact aggregates are more resistant to restructuring (see Sect. 5.5). The validity of this approximation is further addressed in Sect. 5.7.

5.6.5 A complete quantitative description

The mass distribution of the collisional outcome for equal mass colliding projectiles can be constructed using parameters read from Tab. 5.7-Tab. 5.6. Figure 5.24 shows contour plots of the required 4 parameters. Intuitively, the mean mass of

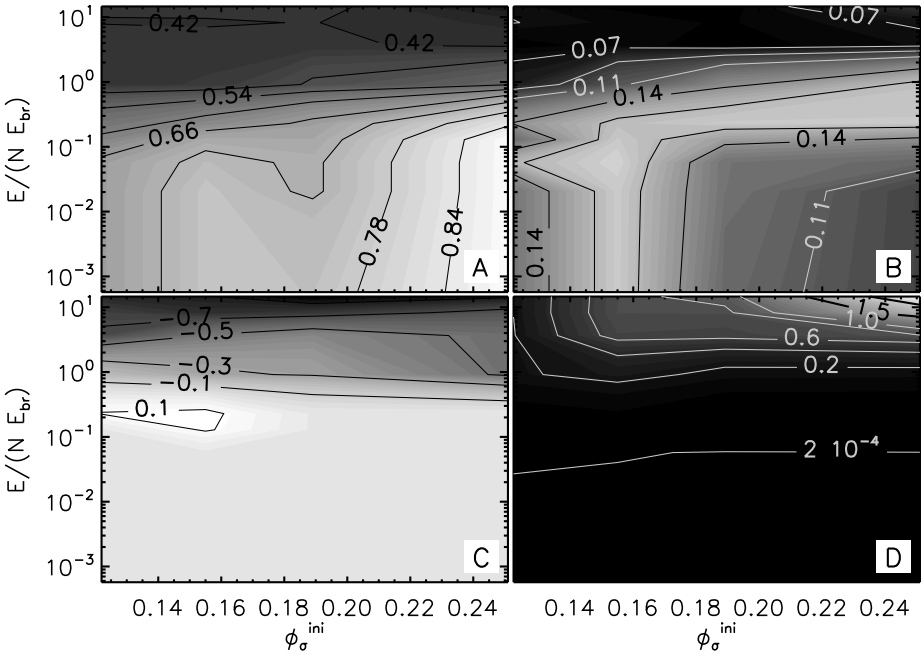

Figure 5.24 — Parameters as a function of the filling factor and impact energy. Mean mass of the Gaussian component (a), width of the Gaussian component (b), slope of the power-law (c), mass ratio of the power-law to the Gaussian component (d).

the large component (upper left panel) decreases with increasing energy. Similarly the width of this component (upper right panel) decreases with increasing energy as a result of fragmentation and grazing collisions. Therefore, an increas-

ing impact energy causes a decrease of the mass of the largest fragment, and the tail of the Gaussian component decreases. This shattered mass shifts then to the small fragments power-law component. This power-law component does not exist at low energies and only large aggregates are produced in this stage due to growth and grazing collisions. Thus the slope of this component (lower left panel) starts to decrease only at larger energies. Note that for a weak erosion, where the slope of the power-law cannot be determined we assume it is $q = 0$.

Figure 5.25 shows compression of aggregates in the global recipe. This contour plot illustrates Tab. 5.9. The low energy collisions cause a decrease of the

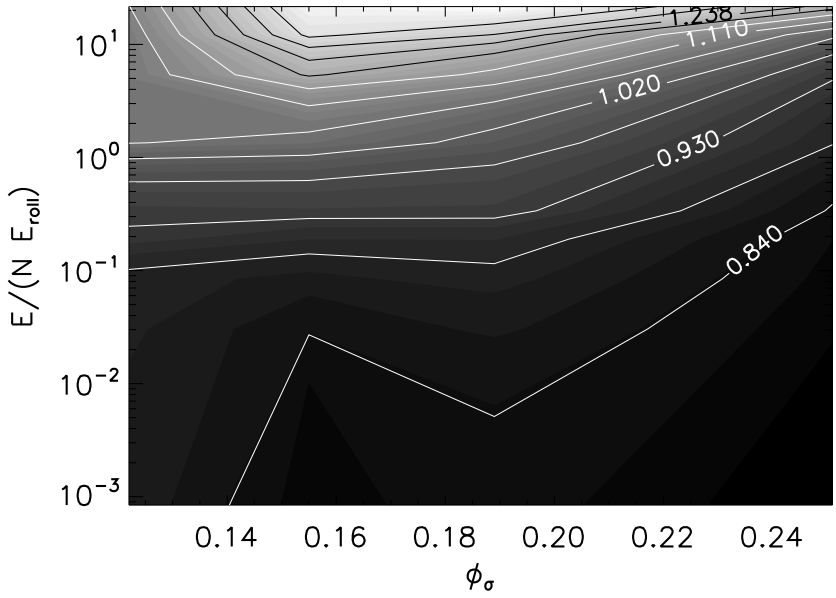

Figure 5.25 — The change of the filling factor ϕ_σ relative to the initial filling factor $\phi_\sigma^{\rm ini}$. Values below unity ($\phi_\sigma/\phi_\sigma^{\rm ini} < 1$) indicate decompaction and values above unity ($\phi_\sigma/\phi_\sigma^{\rm ini} > 1$) mean compaction.

filling factor ϕ_σ for all aggregates. The effect of decompaction is similar for all particles, although the largest decrease of ϕ_σ is observed for the most compact aggregates. Faster impacts result in compression and an increase of the filling factor. Aggregates with the lowest filling factor ϕ_σ show the lowest structural change. The density increases only by a factor of about $\phi_\sigma/\phi_\sigma^{\rm ini} = 1.11$ at the highest energies. For very compact aggregates, at the same energy, this change is somewhat higher ($\phi_\sigma/\phi_\sigma^{\rm ini} = 1.22$). This value is strongly affected by fragmentation. The average largest collision remnant in this case consists of only 0.16 of the total mass. The Maximum compression observed for head-on collisions

at the energy of about $E = N\,E_{\mathrm{roll}}$ reaches only about 0.89 of the initial filling factor. This means that the average largest fragment is decompressed. Fluffy aggregates, both fractal and non fractal, show similar behavior. For these fluffy particles the boundary between decompaction and compression is at the energies of about $E = N\,E_{\mathrm{roll}}$. The filling factor increases further at higher energies. The maximum compression is reached at highest energies. The largest fragment at this energy is about a quarter of the total mass, except of the most fluffy aggregates, that are very difficult to disrupt completely.

Global recipe

In this section we present tables containing the global recipe. They describe both the distribution of fragments (Tab. 5.5, Tab. 5.6, Tab. 5.7, and Tab. 5.8) and the change in the filling factor of the largest fragment, relative to the initial ϕ_σ (Tab. 5.9).

The shape of the distribution of fragment masses depends on the number of contacts that can be broken. The higher the energy is, the stronger and steeper the power-law component is. Therefore the collision energy is normalized to the breaking energy E_{br}. Moreover the energy is distributed globally in the aggregates (hence the name *global recipe*). Therefore the energy is also scaled to the total number of particles N (this is approximately equal to the number of contacts). The first column in each of tables 5.5 – 5.8 shows the normalized energy $E/(N\,E_{\mathrm{br}})$. The following four columns indicate the recipe output quantity (see Tab. 5.4) for aggregates with different initial filling factor $\phi_\sigma^{\mathrm{ini}}$. Table 5.5 presents the slope q of the power-law component of small fragments. The mass normalization can be done with the total mass of colliding aggregates $m_1 + m_2$ and the ratio M_{r} of the mass in this power-law component over the Gaussian component given in Tab. 5.6.

Table 5.5 — The slope of the power-law component.

$E/(NE_{\mathrm{br}})$	$\phi_\sigma^{\mathrm{ini}}$			
	0.122	0.155	0.189	0.251
$5.72 \cdot 10^{-4}$	0.00	0.00	0.00	0.00
$2.06 \cdot 10^{-2}$	0.00	0.00	0.00	0.00
$5.72 \cdot 10^{-2}$	0.00	0.00	0.00	0.00
$1.29 \cdot 10^{-1}$	0.00	0.11	0.00	0.00
$2.29 \cdot 10^{-1}$	0.10	0.12	0.00	0.00
$9.15 \cdot 10^{-1}$	−0.20	−0.28	−0.31	−0.52
$3.66 \cdot 10^{0}$	−0.69	−0.49	−0.42	−0.53
$8.24 \cdot 10^{0}$	−0.73	−0.81	−0.77	−0.65
$1.46 \cdot 10^{1}$	−0.85	−0.89	−1.03	−0.93

The Gaussian component can be reconstructed using three quantities, the ratio of the mass in the two components M_{r}, the mean mass M_{G}, and the width

σ_G. Table 5.7 provides the mean mass, and the width is given in Tab. 5.8.

The change in porosity of aggregates depends on the number of contacts that can roll, as the rolling is the main mechanism responsible for the restructuring. Therefore the energy in the first column of Tab. 5.9 is normalized to the rolling energy E_{roll}. The restructuring also affects the structure of aggregates globally. Thus the collision energy is also normalized to the total number of monomers, which approximates the initial number of contacts. Table 5.9 shows the change in the geometrical filling factor ϕ_σ relative to the initial density $\phi_\sigma{}^{ini}$. This new filling factor represents large fragments from the Gaussian component. The power-law component is simply described by Eq. (5.17).

The difference in energy scaling applied to the part of the recipe describing the fragment distribution and to the part of the recipe providing the compaction accounts for cases of different material properties, where the ratio of the rolling energy E_{roll} to the breaking energy E_{br} may be different than for Quartz. Therefore different physical processes (compaction/decompaction and

Table 5.6 — Mass ratio of the small fragments component (power-law) to the largest fragment component (Gaussian).

$E/(NE_{br})$	ϕ_σ^{ini}			
	0.122	0.155	0.189	0.251
$5.72 \cdot 10^{-4}$	$0.00 \cdot 10^{-0}$	$0.00 \cdot 10^{-0}$	$0.00 \cdot 10^{-0}$	$0.00 \cdot 10^{-0}$
$2.06 \cdot 10^{-2}$	$0.00 \cdot 10^{-0}$	$5.43 \cdot 10^{-5}$	$0.00 \cdot 10^{-0}$	$0.00 \cdot 10^{-0}$
$5.72 \cdot 10^{-2}$	$1.17 \cdot 10^{-3}$	$3.26 \cdot 10^{-4}$	$8.14 \cdot 10^{-5}$	$1.70 \cdot 10^{-4}$
$1.29 \cdot 10^{-1}$	$4.61 \cdot 10^{-3}$	$1.47 \cdot 10^{-2}$	$4.53 \cdot 10^{-3}$	$2.86 \cdot 10^{-3}$
$2.29 \cdot 10^{-1}$	$3.67 \cdot 10^{-2}$	$5.66 \cdot 10^{-2}$	$1.14 \cdot 10^{-2}$	$1.04 \cdot 10^{-2}$
$9.15 \cdot 10^{-1}$	$1.73 \cdot 10^{-1}$	$2.67 \cdot 10^{-1}$	$1.49 \cdot 10^{-1}$	$1.39 \cdot 10^{-1}$
$3.66 \cdot 10^{0}$	$1.91 \cdot 10^{-1}$	$6.83 \cdot 10^{-1}$	$6.63 \cdot 10^{-1}$	$7.87 \cdot 10^{-1}$
$8.24 \cdot 10^{0}$	$2.03 \cdot 10^{-1}$	$7.53 \cdot 10^{-1}$	$7.57 \cdot 10^{-1}$	$1.72 \cdot 10^{-0}$
$1.46 \cdot 10^{1}$	$2.02 \cdot 10^{-1}$	$7.45 \cdot 10^{-1}$	$8.79 \cdot 10^{-1}$	$2.39 \cdot 10^{-0}$

Table 5.7 — Mean mass of the Gaussian component normalized to the total mass.

$E/(NE_{br})$	ϕ_σ^{ini}			
	0.122	0.155	0.189	0.251
$5.72 \cdot 10^{-4}$	0.671	0.756	0.749	0.883
$2.06 \cdot 10^{-2}$	0.671	0.756	0.711	0.883
$5.72 \cdot 10^{-2}$	0.671	0.736	0.711	0.883
$1.29 \cdot 10^{-1}$	0.610	0.697	0.691	0.883
$2.29 \cdot 10^{-1}$	0.575	0.620	0.671	0.829
$9.15 \cdot 10^{-1}$	0.430	0.436	0.485	0.536
$3.66 \cdot 10^{0}$	0.427	0.426	0.423	0.415
$8.24 \cdot 10^{0}$	0.419	0.418	0.421	0.401
$1.46 \cdot 10^{1}$	0.422	0.428	0.436	0.359

erosion/fragmentation) are isolated by different scaling, i.e.,restructuring scales with the rolling energy, while the fragmentation scales with the breaking energy.

Local recipe

The local recipe describe the outcome of a collision between small aggregates and a large target. In the case of the high energy impacts erosion occurs, resulting in the large target aggregate accompanied by the distribution of small fragments. The energy is locally distributed over monomers of the small impactor and surface grains of the target. Thus in this case we scale the energy with the reduced number of monomers $N_\mu = N_1 N_2/(N_1 + N_2)$, which basically is the number of grains in the small aggregate. As the erosion is determined by the number of contacts that can be broken, we scale the collision energy to the breaking energy $E_{\rm br}$.

Table 5.8 — Width of the large fragments component (Gaussian) normalized to the total mass.

$E/(NE_{\rm br})$	$\phi_\sigma^{\rm ini}$			
	0.122	0.155	0.189	0.251
$5.72 \cdot 10^{-4}$	0.124	0.170	0.118	0.098
$2.06 \cdot 10^{-2}$	0.124	0.170	0.123	0.098
$5.72 \cdot 10^{-2}$	0.158	0.175	0.123	0.117
$1.29 \cdot 10^{-1}$	0.120	0.169	0.147	0.137
$2.29 \cdot 10^{-1}$	0.141	0.164	0.170	0.169
$9.15 \cdot 10^{-1}$	0.077	0.107	0.135	0.164
$3.66 \cdot 10^{0}$	0.061	0.065	0.061	0.067
$8.24 \cdot 10^{0}$	0.070	0.066	0.063	0.071
$1.46 \cdot 10^{1}$	0.068	0.062	0.061	0.089

Table 5.9 — A fractional change of the *geometrical* filling factor $\phi_\sigma/\phi_\sigma^{\rm ini}$ averaged over the impact parameter.

$E/(NE_{\rm roll})$	$\phi_\sigma^{\rm ini}$			
	0.122	0.155	0.189	0.251
$8.44 \cdot 10^{-4}$	0.867	0.818	0.837	0.796
$3.04 \cdot 10^{-2}$	0.874	0.843	0.860	0.816
$8.44 \cdot 10^{-2}$	0.877	0.867	0.878	0.822
$1.90 \cdot 10^{-1}$	0.923	0.901	0.902	0.826
$3.37 \cdot 10^{-1}$	0.942	0.944	0.943	0.838
$1.35 \cdot 10^{0}$	1.067	1.053	1.005	0.888
$5.40 \cdot 10^{0}$	1.082	1.206	1.144	0.937
$1.21 \cdot 10^{1}$	1.088	1.322	1.274	1.032
$2.16 \cdot 10^{1}$	1.109	1.368	1.395	1.223

Table 5.10 shows the mean mass that is ejected during a collision relative to the mass of a smaller aggregate. The first column indicates the scaled energy, and the following four columns show the mean ejected mass for collisions of aggregates of different initial filling factor ${\phi_\sigma}^{\rm ini}$. The mass of the cratered target aggregate can then be immediately calculated. Interestingly the third column ($\phi_\sigma^{\rm ini} = 0.09$) shows the effect of the mass ratio on the collision outcome that has been presented in Fig. 5.14a (see Sect. 5.5.2 for a detailed discussion).

In the case of the structure modification the local recipe describes the large target aggregate only, as the filling factor of small fragments can be easily described (see Eq. (5.17)). Bombarding large aggregates with small projectiles results in very small relative change of the filling factor (that of the target particle), as the filling factor quantifies the global structure of the large target aggregate. Therefore in this case the energy scaling should be done in respect to the total number of monomers N, which basically is the number of particles in the larger aggregate. Moreover the restructuring mechanisms is determined by the number of monomers that can roll. Thus the energy is scaled by the rolling energy $E_{\rm roll}$.

Table 5.11 presents the relative change of the geometrical filling factor for the target particle. The energy listed in the first column is normalized to the rolling energy $E_{\rm roll}$ and to the total number of monomers N.

Table 5.10 — Mean ejected mass relative to the projectile mass. The mass ratio of the colliding particles is 0.001.

$E/(N_\mu E_{\rm br})$	$\phi_\sigma^{\rm ini}$			
	0.07	0.09	0.13	0.16
0.23	0.97	0.44	0.52	0.11
0.92	0.98	0.58	0.52	0.11
3.66	1.15	97.6	3.42	0.74
14.6	2.70	109.3	21.3	7.83
33.0	1.21	125.1	30.9	14.7
58.6	2.76	148.0	34.8	26.9

Table 5.11 — Relative change of the filling factor $\phi_\sigma/\phi_\sigma^{\rm ini}$. Mass ratio of the two colliding particle is 10^{-3}.

$E/(N\ E_{\rm roll})$	$\phi_\sigma^{\rm ini}$			
	0.07	0.09	0.13	0.16
0.00034	1.00004	1.00001	1.00005	1.00031
0.00135	1.00002	1.00011	1.00964	1.00072
0.00539	1.00010	1.04656	1.00983	1.00051
0.02155	1.00077	1.05293	1.01031	0.99677
0.04849	1.00012	1.06677	1.01024	0.99314
0.08620	1.00082	1.06368	1.00689	0.98781

5.7 Discussion

The presented recipe provides the quantified outcome of a collision that depends on four parameters

1. The initial filling factor of colliding aggregates $\phi_\sigma{}^{\rm ini}$;
2. The impact parameter;
3. The collision energy;
4. The mass ratio of the colliding aggregates.

Here we present the role that each of these four parameters plays in shaping the outcome of a collision.

5.7.1 Effect of the initial compactness

The structure of aggregates strongly affects the collision outcome. This influence is twofold.

First, the packing density of monomers (i.e.,the filing factor) determines the strength of an aggregate and thus its ability to sustain damage. If a particle is compact, a relatively weak restructuring causes the formation of many new contacts resulting in an increase of a rigidity of an aggregate. Moreover, the packing density can be presented as the *penetration depth*. In the case of compact aggregates voids between monomers are small, and particles are well shielded from projectiles. A monomer trying to reach the center of an aggregate will most likely be scattered in surface layers. The fluffy aggregates on the other hand have larger voids between grains and can be penetrated more easily. Thus if a porous particle is hit by a small aggregate, the chances are that it will break, as a result of fragmentation of the inner region. The reason is that the deep penetration allows the impactor to reach the center of an aggregate and break contacts that hold the *arms* of the aggregate together. In Fig. 5.1 the fluffy particles are made of relatively large and fluffy parts connected together in the central region. Thus the core of a fluffy aggregate is very important to keep the pieces together. If it is shattered, the entire aggregate breaks into several large fragments. Compact particles on the other hand are hard to penetrate and cannot be broken into large fragments. Their surface is eroded instead.

The compactness of an aggregate is also affecting the collision outcome by its ability to redistribute and dissipate the impact energy over a large number of monomers. This "energy coupling" can be expressed in terms of a number of grains that actively participate in a collision. As the processes like rolling and breaking contacts are responsible for energy dissipation, the more particles are involved, the more interactions occur and thus the energy is more efficiently dissipated. Fluffy aggregates with low strength may break easily. Thus the energy sufficient to break a large number of contacts may not be equally distributed over all monomers, as one broken contact might detach a large fragment of the

aggregate. In this case the energy would be distributed over a smaller number of monomers causing severe fragmentation, but only of that detached part.

Therefore it is useful to define an effective number of monomers taking active part in the collision. Konstandopoulas (2000) parameterized it using a rigidity parameter that defines the fraction of the target mass that dissipates the impact energy. Here we determine the effective number of monomers $N_{\rm eff}$ in a following way.

If we take a monomer inside the fractal aggregate and calculate the column density of particles from the center, we get

$$N_{\rm col} \propto N_{\rm tot}^{1-2/D_{\rm f}}, \tag{5.22}$$

which in principle is the number of particle - particle interactions required for the monomer to reach the surface and escape. Assuming that this holds for all particles in the aggregate the total effective number of grains that would be involved in the collision is

$$N_{\rm eff} = C N_{\rm tot}^{2-2/D_{\rm f}}, \tag{5.23}$$

where

$$C = k_{\rm f}^{2/D_{\rm f}} \frac{D_{\rm f}}{4\pi(D_{\rm f}-2)r_0^2}. \tag{5.24}$$

Figure 5.26 shows the largest collision remnant as a function of the impact energy. The two panels show the result with: Fig. 5.26a - energy scaled to the total number of monomers and Fig. 5.26b - the effective number of monomers. The new scaling shifts the data such that curves for collisions of aggregates of the different mass and the different porosity overlap. The fragmentation occurs then at the impact energy of $E = N_{\rm eff}\, E_{\rm br}$. Note that this approach is applicable to head-on collisions only, as the impact parameter introduce an additional effect to the energy distribution within the colliding aggregates.

5.7.2 Effect of the impact parameter

Offset collisions influence both the compaction and fragmentation/erosion of the colliding aggregates. The main reason is that the energy is not transported very efficiently into aggregates. In the case of a central collision the kinetic energy is naturally transported into both aggregates, as the interaction spreads from the center (i.e.,region right in between the aggregates) outwards. The monomers are pushed closer together actively taking part in the energy dissipation. An increase of the impact parameter results in a decrease of the number of grains per unit volume. This means that fewer grains actually collide resulting in a weaker fragmentation.

This behavior is observed both in the restructuring of aggregates and in the fragmentation. Fluffy aggregates are strongly compressed in central impacts, and form very elongated structures in grazing collisions (see Fig. 5.4). More compact aggregates are hard to compress, since the high packing density leads to an increase of contacts preventing any further restructuring. In

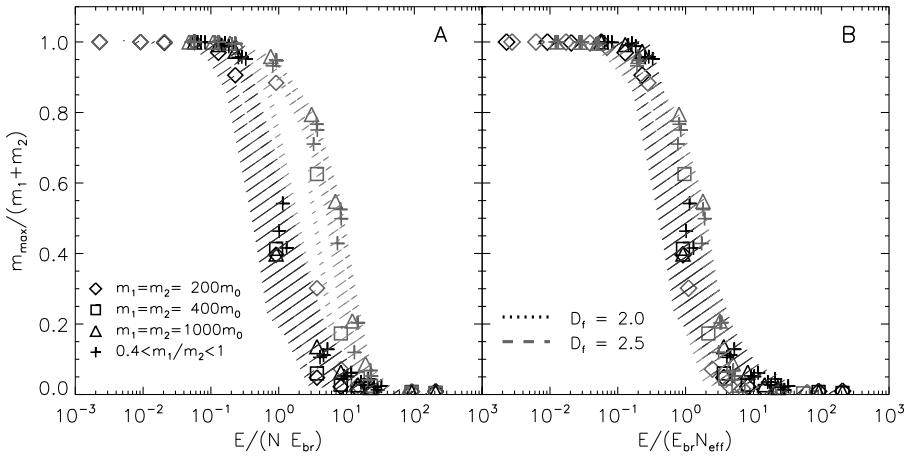

Figure 5.26 — The mass of the largest collision remnant as a function of the collision energy. The impact energy is normalized to the breaking energy times the total number of monomers (a) and to the breaking energy times the effective number of grains $N_{\rm eff}$ (b). Presented are only results of head-on collisions of aggregates of different mass and different porosities.

offset collisions compact aggregates indicate the hit-and-stick behavior as a result of very efficient energy dissipation mechanism. Therefore the outcome of a collision in the sticking energy regime ($E \lesssim 0.1NE_{\rm roll}$) for compact particles is very similar regardless of the impact parameter (see Fig. 5.5). When the collision energy cannot be efficiently dissipated anymore the erosion sets in and restructuring strengthens. In offset collisions aggregates are exposed to tensile forces. Particles produced in central impacts become very compact, while aggregates formed in grazing collisions are elongated (see Fig. 5.9). Monomers are pulled away from each other increasing porosity. A simple example is shown in Fig. 5.27. In this grazing collision at energy of about $E \approx 0.75NE_{\rm roll}$ a string of monomers is pulled out of two compact aggregates. Such aggregates are frequently produced in collisions at large impact parameter. Therefore decompaction is an important mechanisms that strongly influences the structure of aggregates in collisions with large impact parameter.

5.7.3 Effect of the impact energy

The influence of the energy is the most intuitive. Higher energies are directly related to stronger restructuring, erosion or fragmentation. The first restructuring occurs for very fluffy aggregates at energies sufficient to roll one contact. However, this change in the structure is too small to be observed. For it to be visible, a few contacts should be restructured. Therefore the description pro-

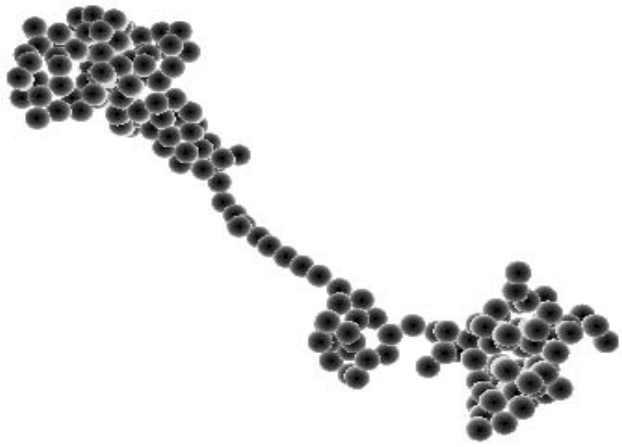

Figure 5.27 — Particle formed in an offset collision of two compact particles at energy of $E \approx 0.75NE_{\mathrm{roll}}$.

vided by Dominik and Tielens (1997) is confirmed in our simulations. Although the degree of compression depends on the initial filling factor ϕ_σ, the maximum compression is reached at energies of about $0.5NE_{\mathrm{roll}}$, which is close to threshold predicted by Dominik and Tielens (1997) and confirmed experimentally by Blum and Wurm (2000). The maximum compression obtained in our study is lower than obtained in a quasi-static compression (Blum et al. 2006; Paszun and Dominik 2008b). This, however, can be an effect of small aggregate sizes, where the filling factor is strongly affected by the porous outer layers (Paszun et al. 2008).

A further increase of the collision energy causes flattening and effectively decompaction of aggregates. Therefore the collisional compaction must not be assumed to be the only process that influences the structure of aggregates, as both grazing collisions and higher energy impacts lead to flattening or stretching of particles.

5.7.4 Effect of the mass ratio

The division of the recipe into the local and the global recipe introduces the mass ratio effects. It is, however, noticeable that mass ratio has an effect in different energy regimes.

The hit-and-stick collisions lead to a different density structure for different mass ratios. In the Brownian growth phase fractal and elongated aggregates are produced. As the mass ratio changes, particles become non fractal (e.g.,the PCA or the hierarchical growth phase). Therefore the structure of an aggregate formed in this regime depends on the mass ratio. The recipe, however, is

focused on collisions at higher energies, where restructuring or fragmentation dominates.

In the restructuring energy regime, the outcome of a collision depends purely on energy, unlike in the hit-and-stick regime. Therefore the mass ratio does not play a major role. The filling factor evolution for collisions of aggregates with different mas ratio is presented in Fig. 5.28. Impacts of small particles

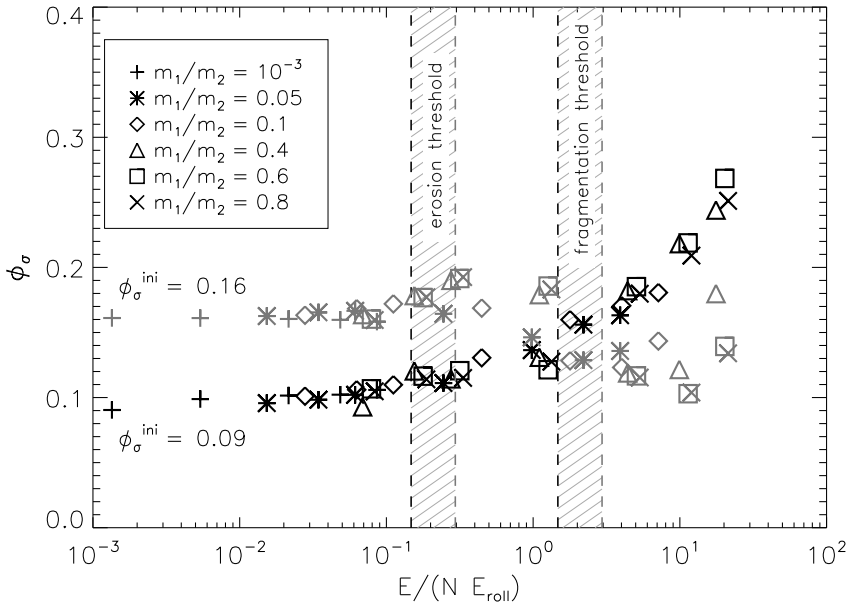

Figure 5.28 — The geometrical filling factor of aggregates produced by head-on impacts of aggregates of different mass on a large target, made of 1000 monomers. Different symbols indicate mass ratio, while colors correspond to fluffy aggregates – black and compact aggregates – grey.

on a larger target influence the filling factor of the large target aggregate. However, regardless of the mass ratio, the filling factor ϕ_σ falls onto a single curve that is common for different cases of the mass ratio. Therefore the filling factor resulting from collisions at energy above the restructuring threshold depends purely on the collision energy. Dashed areas in this plot indicate the onset of erosion (loss of $\sim 0.05N$ monomers) and fragmentation (loss of $\sim 0.5N$ monomers). The dashed area indicates the range in the energy, as the erosion and the fragmentation thresholds are different for aggregates with different filling factor ϕ_σ. Above the erosion threshold compression still occurs, although some monomers are ejected from the aggregates. Above the fragmentation threshold, however, the aggregate size drops very fast (cf. Fig. 5.11 & Fig. 5.26) and the filling factor

is strongly influenced by the size of particles (at the highest energy the largest fragment is made of several monomers only).

The fragmentation threshold sets the limit, where the collision outcome is independent of the mass ratio (cf. Fig. 5.23). However, impacts at lower energies may result in very different outcome for large mass ratio and for equal mass collision partners. In the first case (large mass ratio) the energy is distributed locally in a big target aggregate and the dissipation occurs "on site" leading to erosion. Two large aggregates can redistribute the energy over a large number of monomers causing sticking without erosion.

5.7.5 Limitations of our method

Our parameter study covers an extensive parameter space and provides the collision outcome for a wide range of different cases. We provide scaling that allow the presented recipe to be applied for different material properties (i.e.,monomer composition and size), aggregate masses N, and a wide range of energy and structural parameters. To provide a complete picture we present here a list of limitations that will be addressed in the future.

- **The size of aggregates and bouncing.** Although we simulate aggregates of different sizes, the explored mass range covers only rather small particles, made of a few thousands of monomers. This limitations is currently hard to overcome as the simulations of a large number of monomers are computationally very demanding. Although we provide scaling that can be used to extrapolate the recipe to larger sizes, one must apply the recipe with caution. Very large aggregates ($> 100\,\mu$m) studied in experiments can bounce (Langkowski et al. 2008a). This behavior has never been observed in our simulations. Although this is an important effect that significantly affects the growth of dust aggregates, it is still poorly understood.
- **The structure of aggregates.** To provide a simple, quantitative recipe for the collision outcome, we use only one structural parameter: ϕ_σ. It describes the average packing density of monomers in an aggregate. However, the filling factor ϕ_σ can be identical for aggregates of different structure, e.g.,PCA and fractal particles with the fractal dimension $D_\mathrm{f} \sim 2$. Therefore the output of the recipe always assumes a spherical symmetry, even though stretched, elongated aggregates are observed in our simulations, especially at large impact parameters.

The presented bounds of the recipe are expected not to affect the growth of aggregates if the size of aggregates is limited to about $\sim 100\,\mu$m.

5.8 Conclusions and future work

In this work we present results of the extensive parameter study of collisions of three-dimensional aggregates. The outcome of a collision is provided in terms of

the mass distribution of fragments as well as the structure of the produced particles. These simulations agree with the experimental results in this size regime and provide scaling that allows for extrapolation to slightly larger sizes as well as different material properties of monomers (i.e.,composition and size of individual grains).

Our simulations indicate new important mechanisms that influence both the structure and the mass distribution of aggregates:

- The restructuring of aggregates depends mainly on the collision energy. The compaction is reserved for head-on impacts, while offset collisions produce elongated and decompacted particles.
- In the case of erosion and shattering the structure of small fragments is provided in a very simple form (see Eq. (5.17)) regardless of the initial compactness of colliding aggregates or the impact energy.
- The mass distribution of particles produced in a collision consists of two individual components. The power-law distribution of small fragments is accompanied by a strongly pronounced component of large fragments.
- The shape of the mass distribution for the collision outcome averaged over the impact parameter is generally independent of the impact energy for slow collisions. At high energies, however, the shape of the distribution is almost independent of the structure of the colliding particles.

These points are combined together in a form of the recipe that provides the quantitative outcome of a collision. This recipe is formulated in a simple way that can be easily applied to models of dust coagulation in various environments (e.g.,molecular clouds or protoplanetary disks).

Acknowledgment

We thank Jürgen Blum for useful discussions and hospitality during several visits. We also thank Michiel Min for providing us the routine producing the fractal aggregates and Chris Ormel for useful discussions that significantly improved the final shape of the recipe. We acknowledge SARA super computer center for access to the Lisa computer cluster, which made this parameter study possible. We also acknowledge a financial support of Leids Kerkhoven-Bosscha Fonds. This work was supported by the Nederlandse Organisatie voor Wetenschapelijk Onderzoek, Grant 614.000.309.